Fall 2008

Study of the Influence of Nacelle and Pylon on Aerodynamics of a New VU Design

Romain Larose
Embry-Riddle Aeronautical University - Daytona Beach

Study of the influence of Nacelle and Pylon on Aerodynamics of a new VLJ design

by

Romain Larose

A Thesis Submitted to the Graduate Studies Office in Partial Fulfillment if the Requirements for the Degree of Master of Science in Aerospace Engineering

Embry-Riddle Aeronautical University
Daytona Beach, Florida
Fall 2008

Study of the influence of Nacelle and Pylon on Aerodynamics of a new VLJ design

by

Romain Larose

This thesis was prepared under the direction of the candidate's thesis committee chairman, Dr. Magdy Attia, Department of Aerospace Engineering, and has been approved by the members of his thesis committee. It was submitted to the Aerospace Engineering Department and was accepted in partial fulfillment of the requirements for the degree of Master of Science in Aerospace Engineering.

THESIS COMMITTEE:

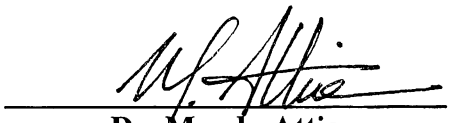

Dr. Magdy Attia
Chairman

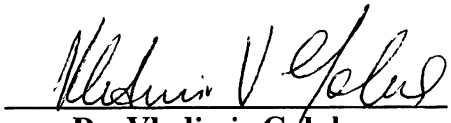

Dr. Vladimir Golubev
Member

Dr. Eric Perrell
Member

Dr. Habib Eslami, Department Chair — **Date** 12/12/08

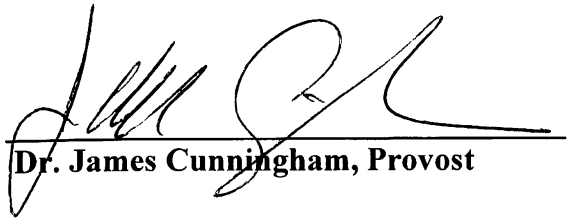

Dr. James Cunningham, Provost — **Date** 12/12/08

ACKNOWLEDGEMENTS

The author would like to acknowledge the help and support of his advisor Dr. Magdy Attia, as well as Dr William Engblom for sharing his experience in Computational Fluid Dynamics.

ABSTRACT

Author: Romain Larose

Title: Study of the Influence of Nacelle and Pylon on Aerodynamics of a new VLJ design

Institution: Embry-Riddle Aeronautical University

Degree: Master of Science in Aerospace Engineering

Year: 2008

The purpose of this thesis was to illustrate the influence of the nacelle and pylon on aerodynamics of a new Very Light Jet design, using Computational Fluid Dynamics.

The objective of the first phase was to repair the existing CATIA model in order to facilitate the meshing process.

The second and third phase was to create two meshes: a mesh for the complete model (aircraft with nacelle and pylon), and a second for the aircraft alone.

The two problems have been solved at cruise conditions using Navier-Stokes equations with a second order accuracy.

The model complying with theory, the results have been then processed.

The analysis resulted in showing that shock waves were forming at the pylon, generating noise, vibration and more drag. Some improvements were discussed needing further investigation.

TABLE OF CONTENTS

LIST OF TABLES

LIST OF FIGURES

1. INTRODUCTION

1.1. Literature Survey

1.1.1 Study of nacelle influence of the ERJ-145

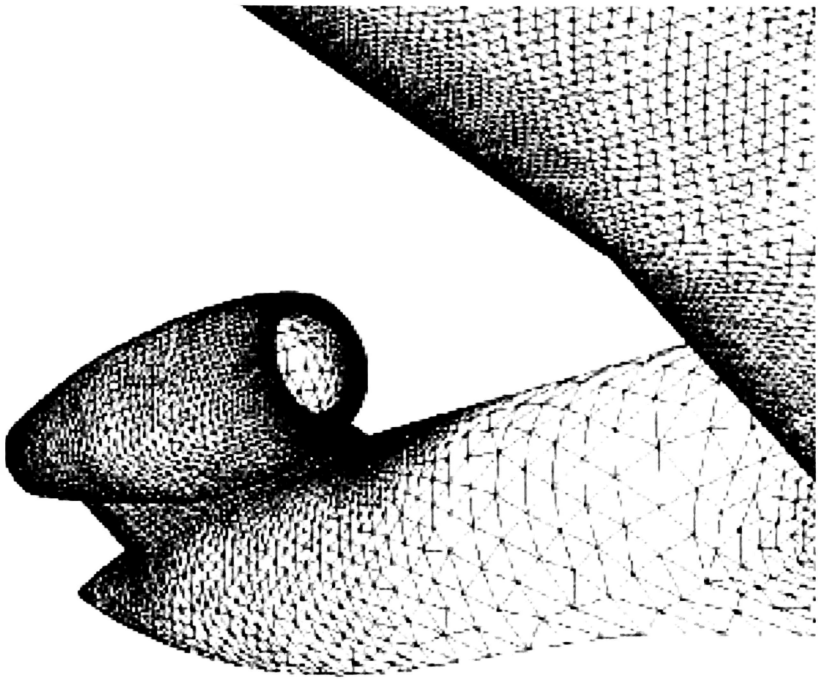

Figure 1: Mesh of the nacelle on the early configuration of ERJ-145

Empresa Brasileira de Aeronáutica, EMBRAER, well known for its ERJ-145, concluded the need for a regional jet aircraft capable of transporting from 30 to 40 passengers. The new EMBRAER ERJ-135 is a 37-seat commuter jet that embodies the EMBRAER "jet family" concept.

The ERJ-135 is mainly based on the ERJ-145, with a fuselage 11.6 ft shorter. EMBRAER engineers saved a considerable amount of money and time by using computational fluid dynamics (CFD) simulation to prove that flow characteristics of the ERJ-135 are very similar to the already-certified ERJ-145.

To proceed, the engineers selected the RAMPANT CFD software package from Fluent Incorporated, which is an efficient finite-volume code based on fully unstructured meshes. To

create the mesh, they used Fluent's TGrid, an automatic mesh generator. They also used the RAMPANT solution-adaptive mesh refinement tool which automatically adapts the grid based on the gradients of the solution.

Pressure inlet boundary conditions were used to define the exhaust flow (set normal to the boundary at the nacelle exhaust) and static pressure boundary conditions at the inlet of the engine. The inlet of the engine was modeled up to the first set of fan blades.

The final grid contained approximately 410,000 tetrahedra.

Euler equations were used (inviscid) and the flow calculations were performed on a Silicon Graphics Origin 2000 server from EMBRAER, with two R10000 processors, and 768 MB of RAM.

1.1.2 Nacelle Impact on Wing & Fuselage of the ARJ21

Computational Fluid Dynamics (CFD) has played a role in the development of the advanced regional jet ARJ21 from China's AVIC 1 Commercial Aircraft Company (ACAC). At ACAC, FLUENT was introduced during the pre-development phase, and it continues to play a major role in design, engine selection, and to save time spent on wind tunnel tests.

Before applying the turbulent Navier-Stokes equations to the complete aircraft, validations were performed on a simplified geometry. Using a 3D wing-body model, predictions of pressure and lift coefficient were compared to experimental data, and very good agreement was obtained. These results gave the engineers confidence in CFD, and its use has expanded to include many components and aspects of the full-scale aircraft.

As an example, the flow above the joint that is formed between the wing and body of an aircraft has been examined. The flow in this region can separate, and if it is possible to reduce or

eliminate the size of the separation region by design modifications, the flight performance of the plane can be improved.

Engineers at ACAC have used FLUENT to study a rear-mounted nacelle configuration, in which the aircraft's engines are installed behind the wings. In this configuration, the position of the nacelle or the design of the wing can cause the wake of the wing to be entrained by the engine, compromising its performance. Using FLUENT, the pressure distribution on the wing for several different rear-mounted nacelle positions has been computed for a flight Mach number of 0.78 at an altitude of 35,000 feet.

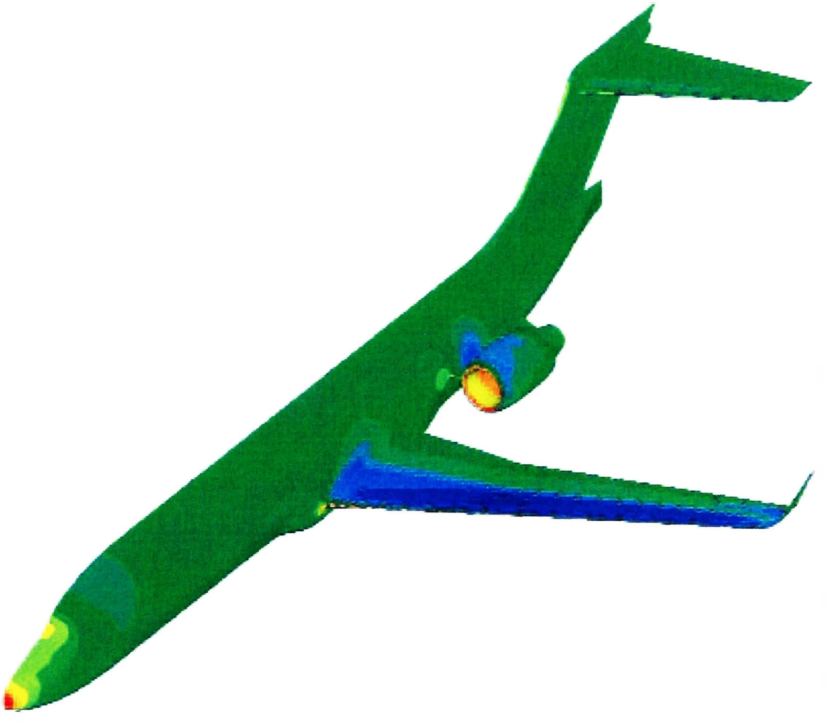

Figure 2: Static pressure on the surface of the ARJ21

The results showed that the lift coefficient of the wing with this configuration is lower than that of a clean wing (without the interference of the nacelle). The drag coefficient is also lower, however, so that the lift/drag ratio is increased. Furthermore, the interference caused by rear-mounted nacelles makes the nose-down pitching moment decrease and it can reduce the trim drag produced by the elevators. The overall analysis of drag indicates that the existence of a

rear-mounted nacelle will have little influence on friction drag, but can have the advantage of reducing the pressure drag.

1.2. MS 760B ParisJet II

The aircraft studied in this project is based on the MS 760B ParisJet II, which was the updated version of the MS 760A ParisJet. The MS 760A was designed primarily by René Gauthier as a four-seat high-speed communications aircraft but was also easily adaptable for training and other duties. It was a derivative of the MS755 Fleuret who lost the military trainer competition against the Fouga Magister in 1953. The Paris Jet was initially known as the MS 760 Fleuret II.

The first flight took place on July 29th 1954 with Jean Cliquet at the controls. The prototype MS 760A ParisJet I had a low wing and was powered by a pair of 880 lbst Turboméca Marboré II turbojets, mounted side by side in the fuselage. It was recognizable by its T shaped vertical stabilizer and by its retractable tricycle landing gear.

The aircraft had four seats, two in the front and two in the back. It was purchased by the French Air Force, Navy, and by several countries worldwide like Brazil and Argentina (48 planes were license built at Cordoba in Argentina).

In 1961 production plants started the manufacturing of the MS 760B ParisJet II, fitted with two Marboré IV 480kg engines, wingtip fuel tanks, an air conditioned cockpit and a bigger luggage compartment.

Customers feedback on the ParisJet II pointed primarily at the difficulty of embarking passengers into the canopy, the lack of real doors was sometimes problematic, particularly for female passengers.

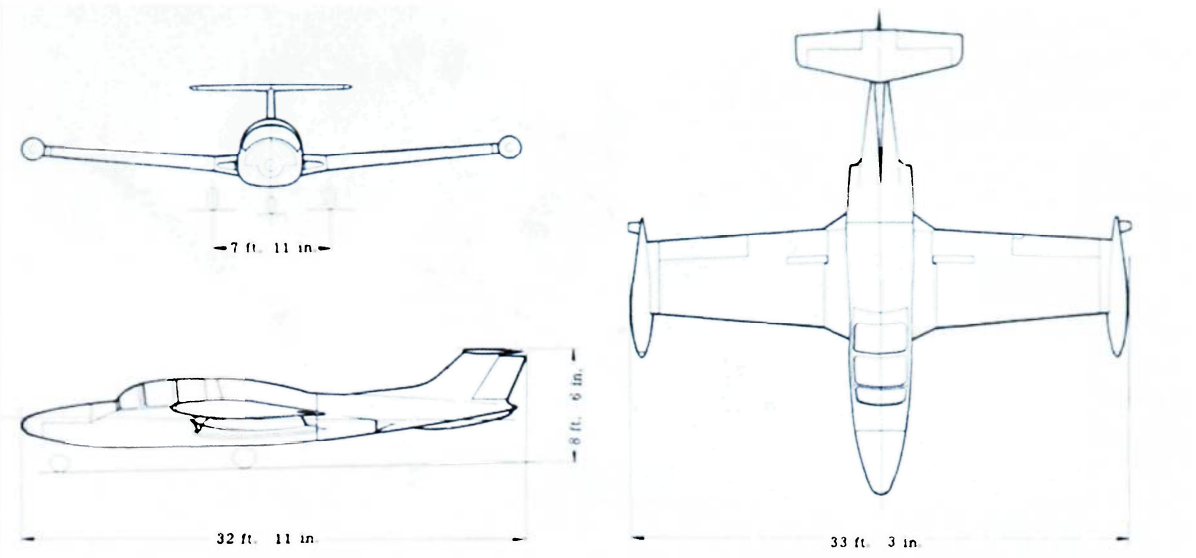

Figure 3: Dimensions of the ParisJet II

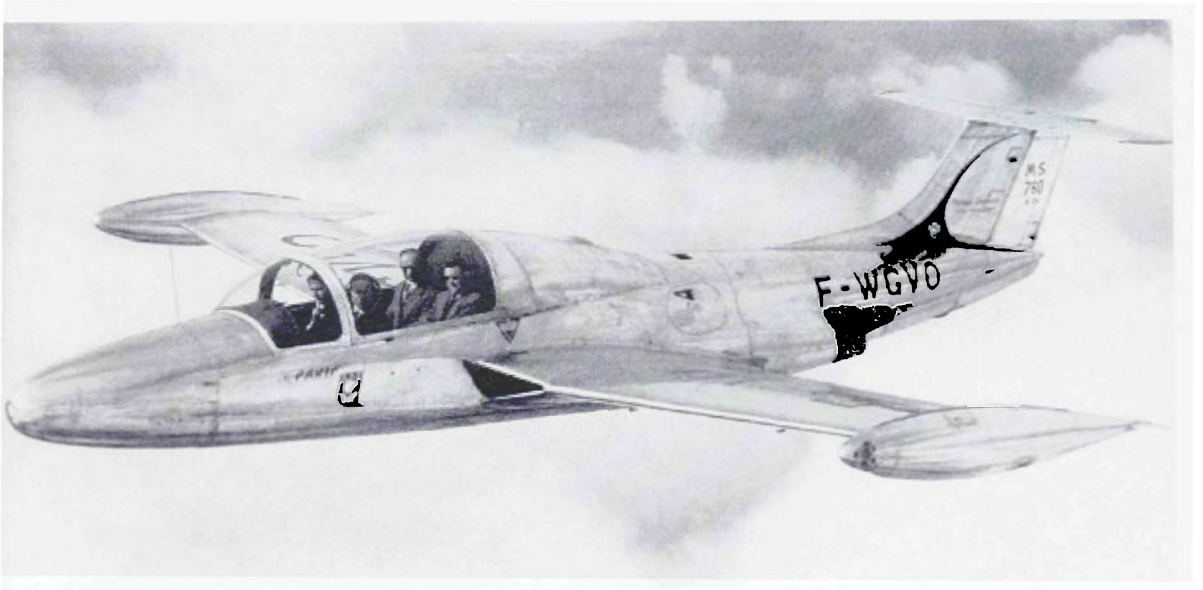

Figure 4: MS 760B ParisJet II

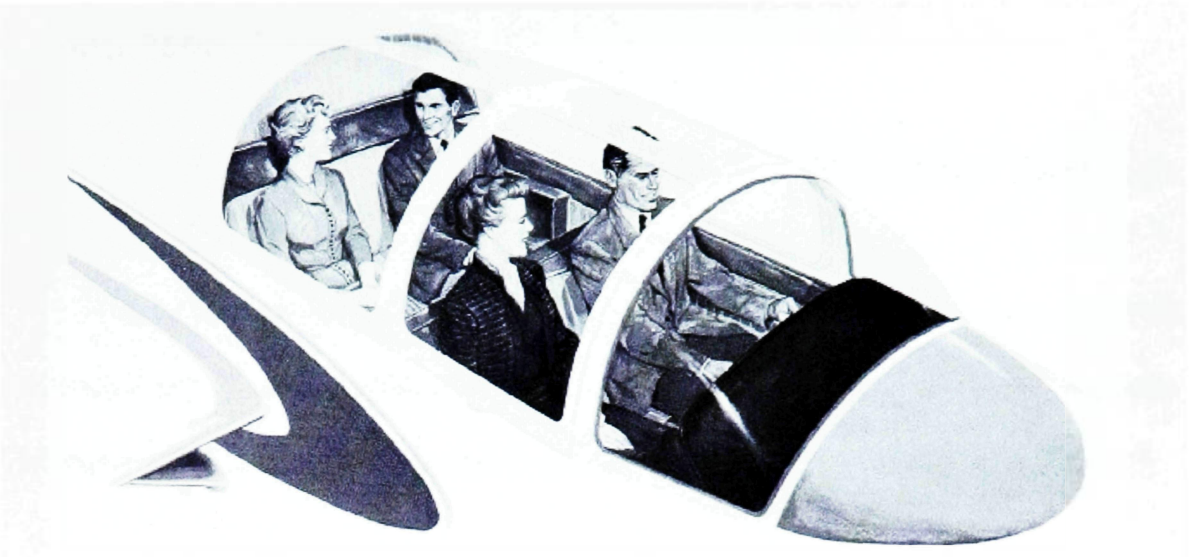

Figure 5: ParisJet II Cabin

CHARACTERISTICS	English Units	SI Units
LENGTH	33 ft 3 in	10. 15 m
WINGSPAN	33 ft 59 in	10. 24 m
HEIGHT	8 ft 53 in	2. 60 m
WEIGHT	4 657 lb (min)/ 8 779 lb (max)	2 070 kg (min)/ 3 902 kg (max)
WING AREA	193. 7 sq ft	18 m^2
CEILING	39 369 ft	12 000 m
MAX SPEED	431. 9 mph	695 km/ h
INITIAL CLIMB RATE	2 460 ft/mn	750 m/mn
MAX RANGE	922 nm	1 740 km
POWER	2 x 1 058 lbs	2 x 480 kg

Table 1: ParisJet II Characteristics

1.3. MS 760C ParisJet IV

The MS 760C ParisJet IV is a new design based on the MS 760B ParisJet II. The goal was to update the ParisJet II using new engines.

Indeed, since the 50's, a huge improvement has been made in engine performance. The new engines are more robust, efficient, and less pollutant. After a quick study, the WILLIAMS FJ33 engine (1500 lbf) has been selected to replace the Turboméca Marboré IV of the ParisJet II.

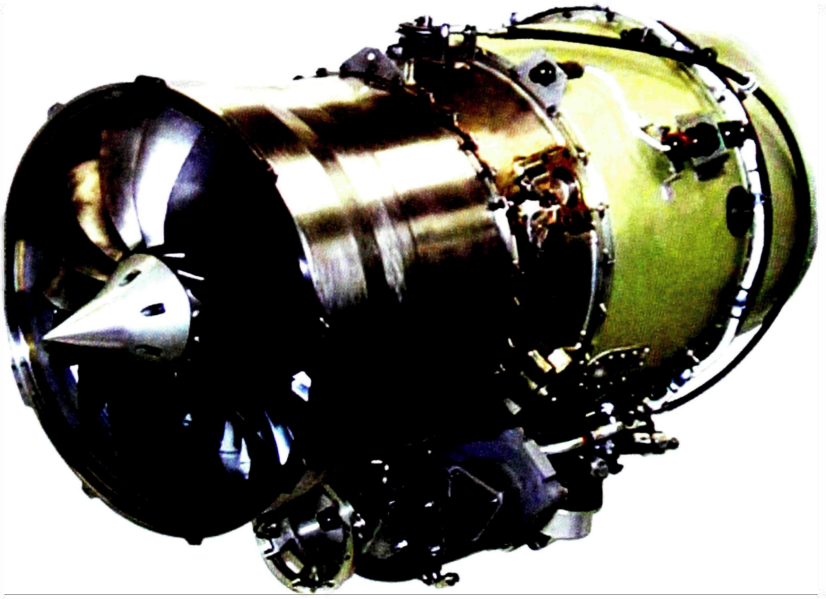

Figure 6: Williams FJ33

The problem with the Williams is that they could not fit inside the fuselage. Hence, the idea of putting the engines in nacelles outside came out. After a quick analysis, both structural and aerodynamic, a new design was done: a system of pylon and nacelle located a little aft the wing on the upper part of the fuselage has been created. In this new design, the leading edge of the wing (was the inlet duct) and the old exhaust have been closed "smoothly".

The following table describes some theoretical characteristics of this ParisJet IV.

CG position	Ref	C_L at 2°	C_D at 2°	C_M at 2°
x_{CG}= 4.07 m (From Nose)	S_w=18 m²	0.2083	0.02173	-0.01814
z_{CG}= 0.339 m (Above Fuselage CL)	MAC= 1.9m			

Table 2: ParisJet IV Theoretical Characteristics

1.4. Process

To fulfill the requirements of this project (and especially time requirements), two cases have been studied and compared: the 2° Angle of Attack case for both a grid without the nacelle and one complete.

The process starts with the CATIA model of the new design. It was already created, but in such a way that the process would have been too complicated or even impossible to finish given the deadline of this project.

Hence, the first step was to repair this model, making it simpler and smooth in order to make the meshing process easier. Then, the model has been cut in half to reduce the calculation time (the problem is symmetric along the fuselage centerline of the aircraft).

The next step was the meshing for the complete model first, using an unstructured grid with Gridgen. Once this mesh created, the nacelle and pylon parts have been deleted to create the grid for the second case.

To run the calculations, FLUENT 3D solver has been used. To run such a huge model (3.3 million cells), the parallel processing feature has been widely used.

Finally, a discussion on this new design has been done and improvements suggested.

2. CATIA Model

2.1. Model Characteristics

Figure 7: Catia Model

2.2. Original 3D Model

The first CATIA model was made by using several plans of section from the original MS 760B ParisJet II. These sections were joined together, creating discontinuous curves. Then, all the changes were applied: closing the leading edge inlet, closing the engine exhaust at the back part of the fuselage and adding pylon and nacelle. This model was finally made of more than 500 surfaces.

All of this leads to a lot of high curvatures problems and gaps which interfere with the real aerodynamics of the aircraft. That is why some repair had to be done. The following figures show such shape problems.

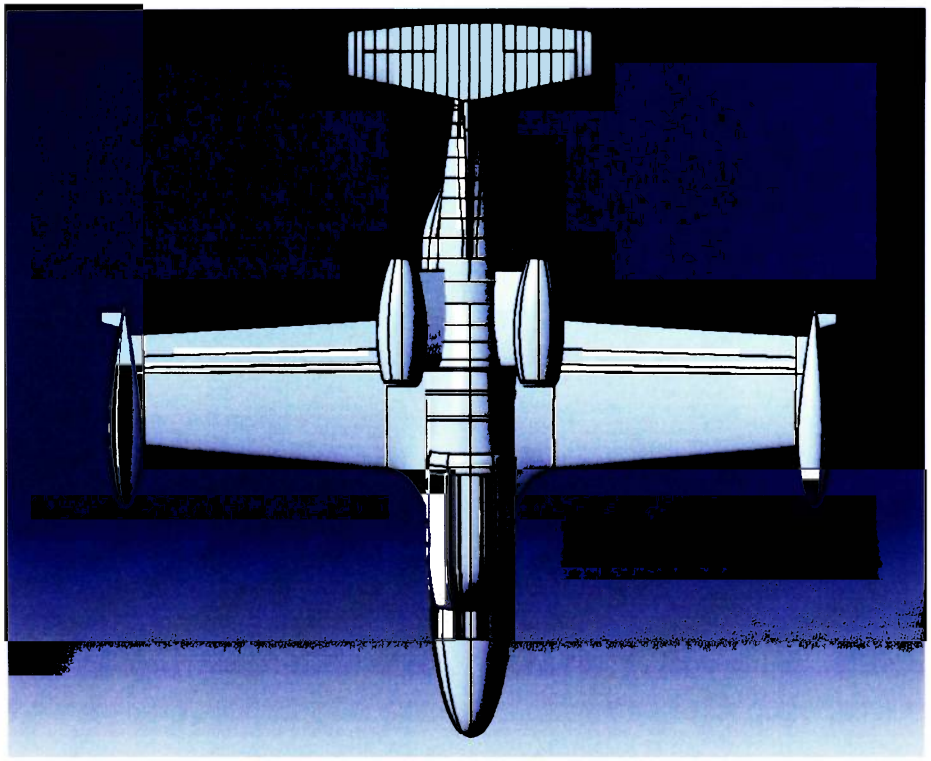

Figure 8: Original Model - Top View

On the figure above, one can see the different sections used to create the model. A close-up on the fuselage is shown on the figure below (without canopy).

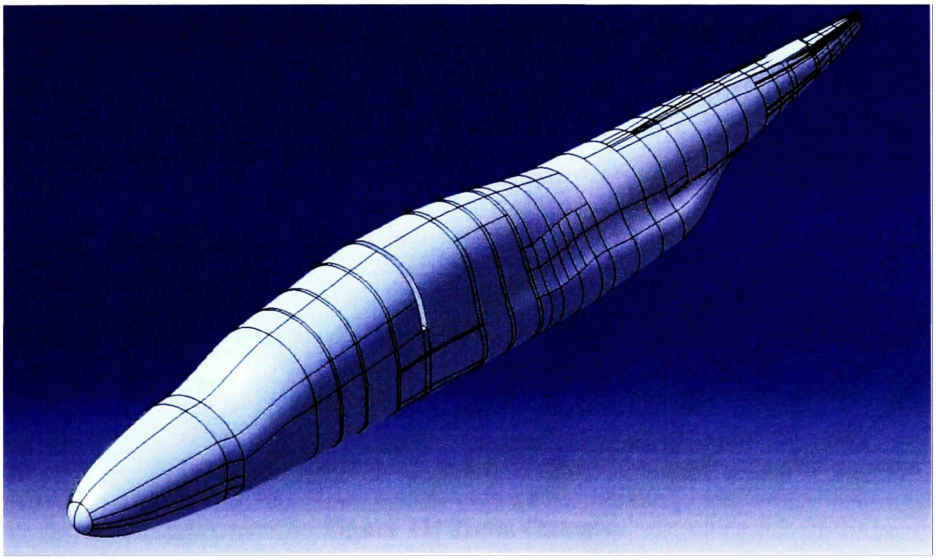

Figure 9: Original Model – Fuselage

The following figure shows an example of discontinuity along the fuselage:

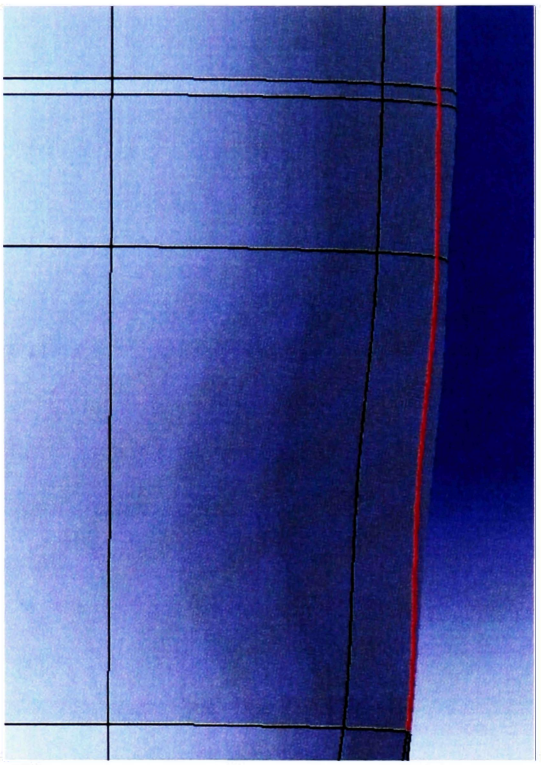

Figure 10: Smoothing problems on Fuselage

The intersection of these unsmoothed surfaces with the canopy is shown in the figure below, and will cause problems while importing the model in the meshing program.

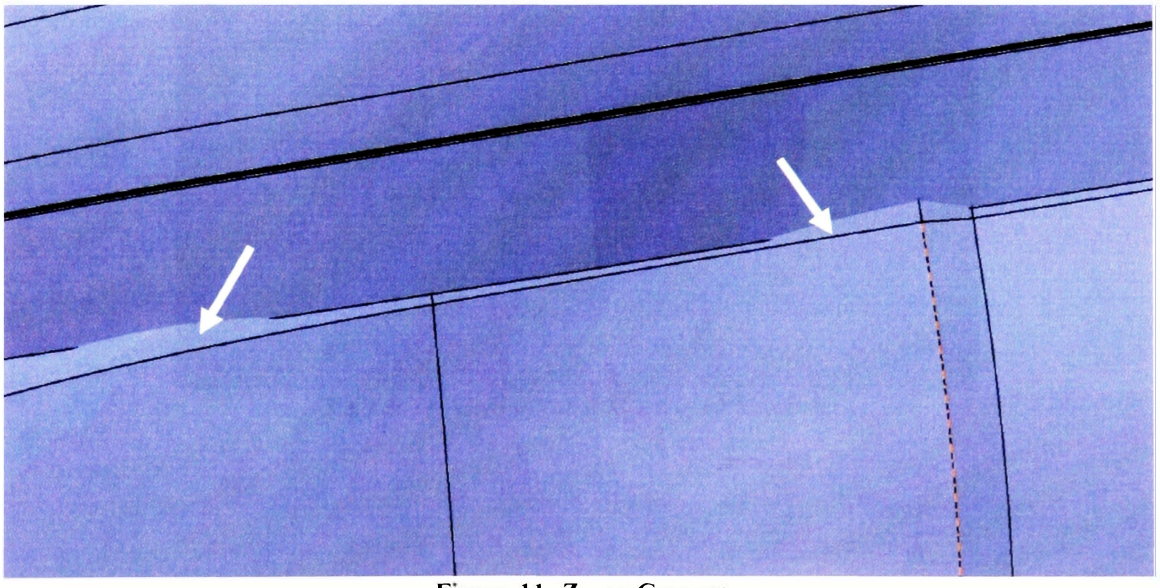

Figure 11: Zoom Canopy

Here are some zoom-in figures showing the geometry defaults involved by the closing exhaust:

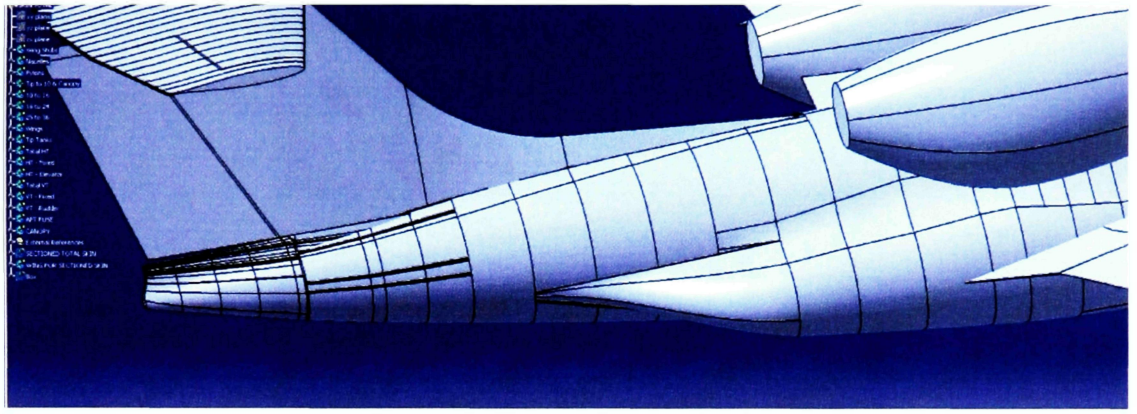

Figure 12: Exhaust Original Model

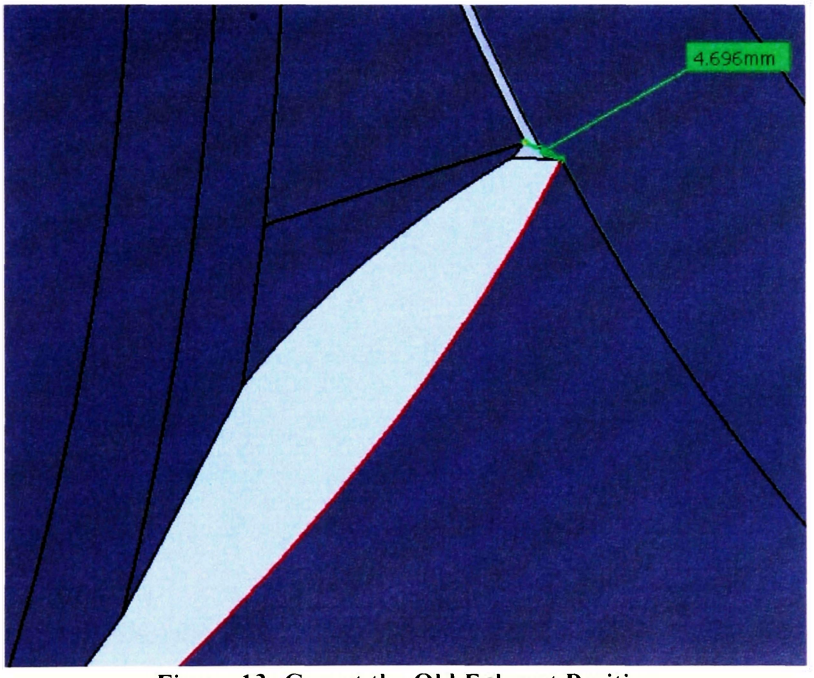

Figure 13: Gap at the Old Exhaust Position

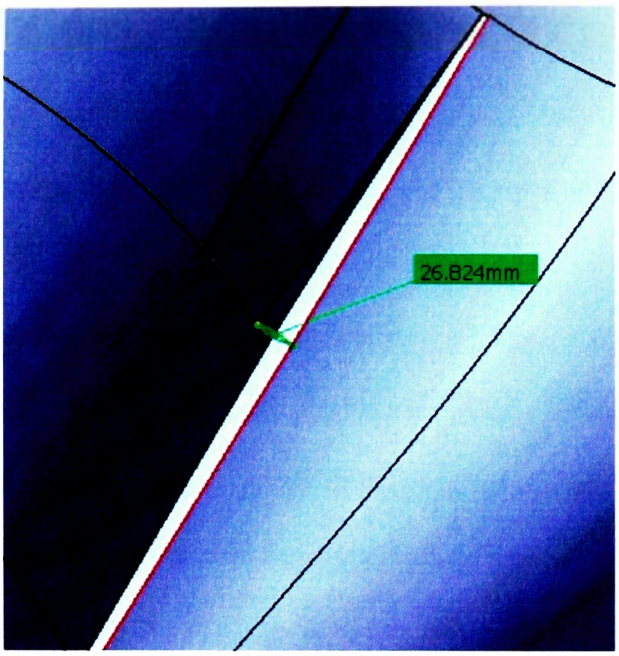

Figure 14: Gap at the Old Exhaust Connection

Figure 15: Gap at the Tail Root

All these geometry problems will lead to linking problems or errors while importing the model into the meshing software. In order to solve these problems, a solution would be to smooth all the surfaces and merge them together. The process is detailed in the next section.

2.3 Repairs

Given the way the model had been created, no extra smoothing was possible as the original designers had already made their best for it. So, the idea of redoing the surfaces came out.

To make it easier, the existing sections have been copied as a sketch, and then scaled in average 0.01 inch bigger all around (maximum of 0.5 at the old exhaust position). This process can be roughly imaged as putting a "plastic wrap" all around the fuselage. Such a small change in dimension is truly negligible. Indeed, 0.01 inches represents an order of magnitude of around 10^{-5} compared to the aircraft length (383 in). 15 to 30 points have been used to define every new half section.

The following figure shows one of these sections:

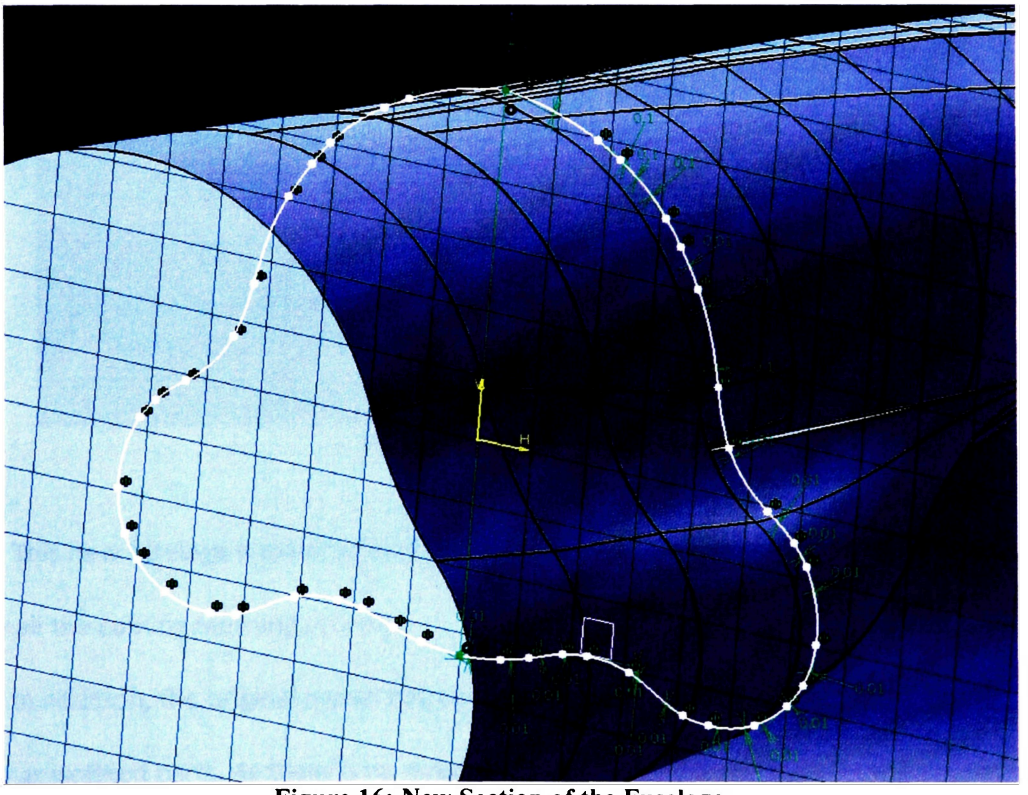

Figure 16: New Section of the Fuselage

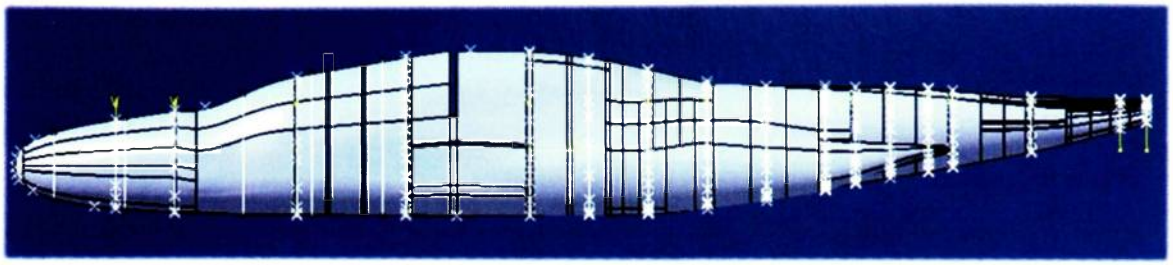

Figure 17: Sections used to create the new fuselage

The location of every newly created section is illustrated in Figure 17. Once they are all created, a high degree polynomial fitting surface is formed.

The following figure shows the fuselage newly created:

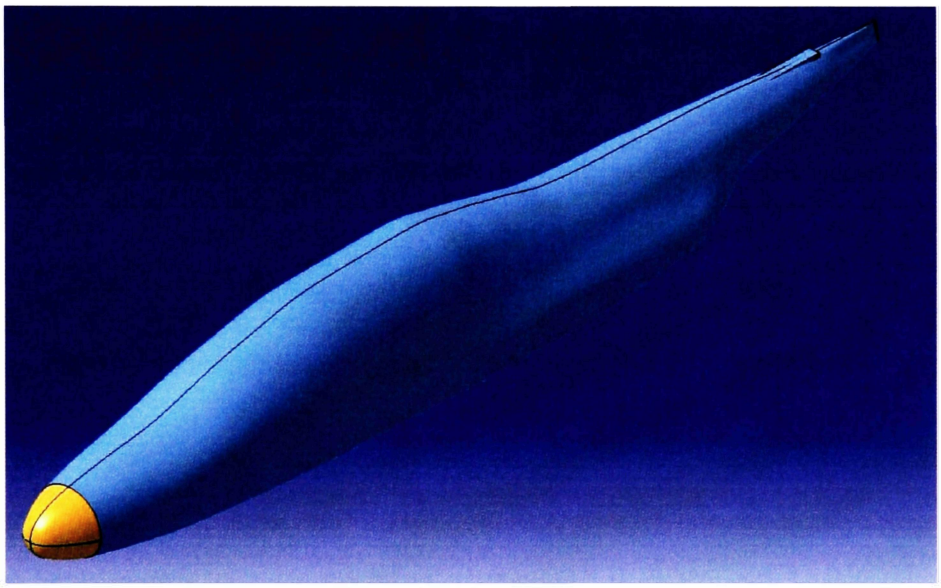

Figure 18: New Fuselage

This new fuselage is made of only two main smooth surfaces - instead of 350 - which simplify all the coming meshing process.

In addition, the original model has been made with the rudder, the elevators and ailerons as isolated parts. As there is no need to move the control surfaces for this problem and also because there were creating gaps at the different hinge lines, the same process has been applied to the wing, the horizontal and vertical tail.

The tip tank fin has been poorly created with surfaces intersecting each other. This caused problems while meshing: the same process has been applied on it too.

Finally, this process has been applied to all the parts of the aircraft, except the pylon, nacelle and tip tank.

Concerning the canopy, its shape was too complicated (too many surfaces, always difficult to use in a meshing program) and created an unclean intersection with the fuselage. It has been completely redone in a simpler manner.

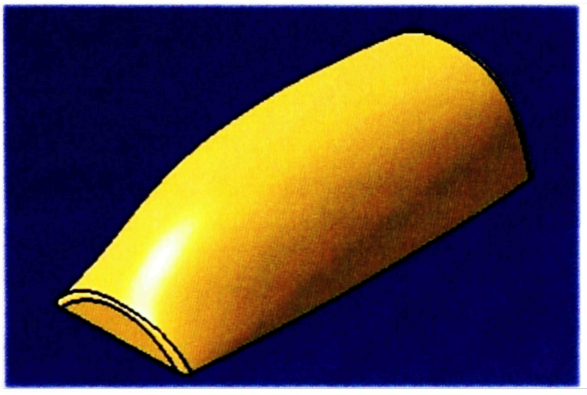

Figure 19: New Canopy

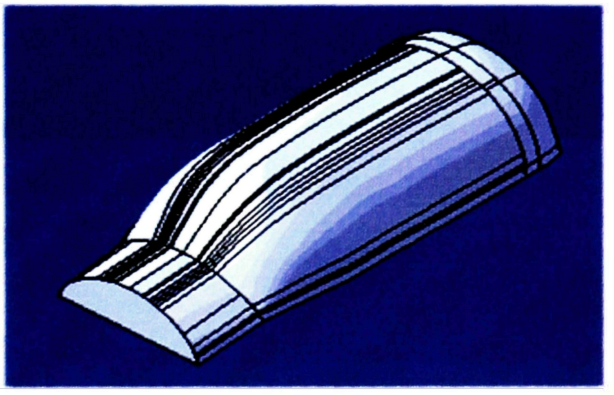

Figure 20: Old Canopy

The final model is shown in the following figures:

Figure 21: Repaired Model - Iso view

Figure 22: New model - Front View

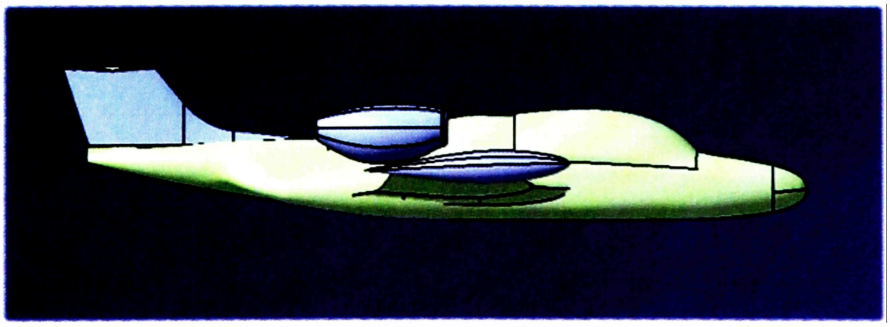

Figure 23: New Model - Left View

This new model is made of only 103 surfaces. The original one contains 510 surfaces.

To reduce the computing time and to simplify the process, the model has been cut in half as there is a plan of symmetry XZ.

3. MESHES

The meshes have been generated using Gridgen. This software, widely used in industry, offers a lot of features. It is one of the most polyvalent (around 40 different solver export types of file available), and is also relatively easy to use and powerful.

An unstructured type of grid has been chosen for several reasons. First, the setup time is a lot reduced compared to structured grid. As this project had to be done in less than a year, the choice has been made that way. In addition, unstructured grids are very suitable for complex geometries and enable more efficient parallelization. Finally, unstructured grids give similar accuracy compared to structured grids.

The grid created does not include extrusions to control every domain shape, and to make it easy to modify or redo the blocks. Moreover, the geometry is too complex in some regions to use that feature.

3.1 Complete Grid

The mesh has been done in a way so that the cells can be concentrated in the regions of interest only, and easy to modify. Hence two different regions have been created in the meshed space around the aircraft.

The first one is directly touching the aircraft. It is made of 11 blocks isolating the different areas of interest (e.g. canopy, nacelle and pylon, wing ...).

The second one surrounds the first region and defines, at its boundaries, the free stream. It is made of 4 coarse grid blocks, split as shown on Figure below.

The whole mesh contains 3.25 million cells.

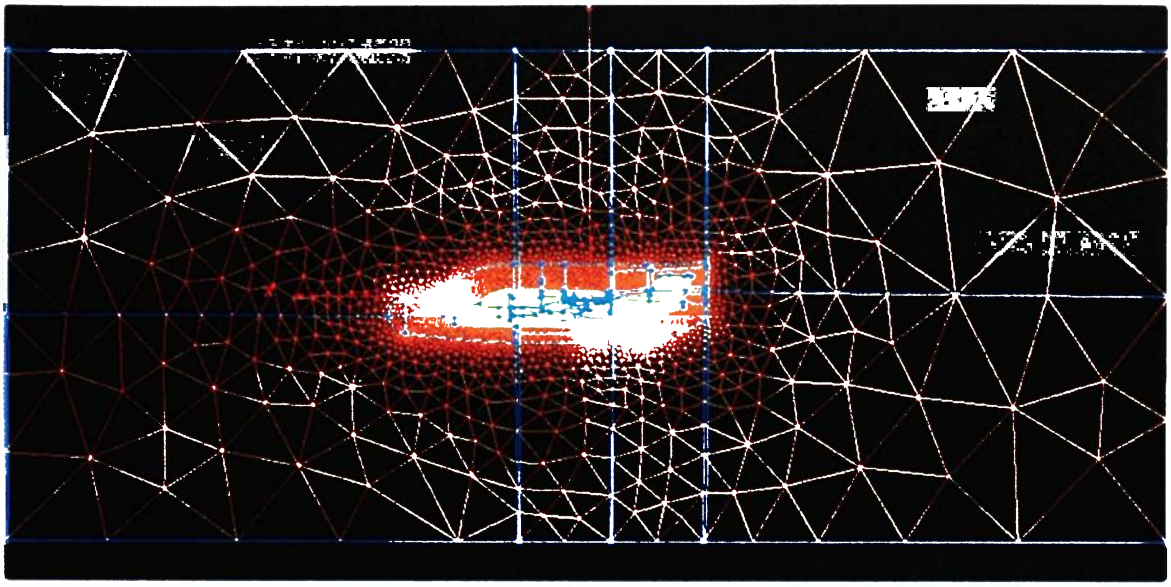

Figure 24: Grid XZ

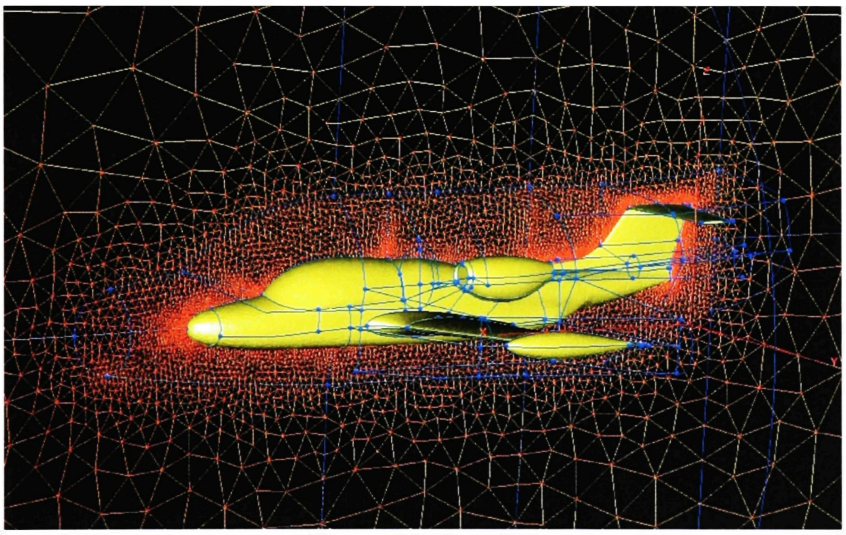

Figure 25: Two different regions

The next sections will describe the blocks of interest.

3.1.1 Grid defining the aircraft

The spacing of the inner triangles is different as one can see on the figure below. A better grid (meaning finer) is needed only in the areas of interest: pylon, nacelle, inlet, outlet, top wing root.

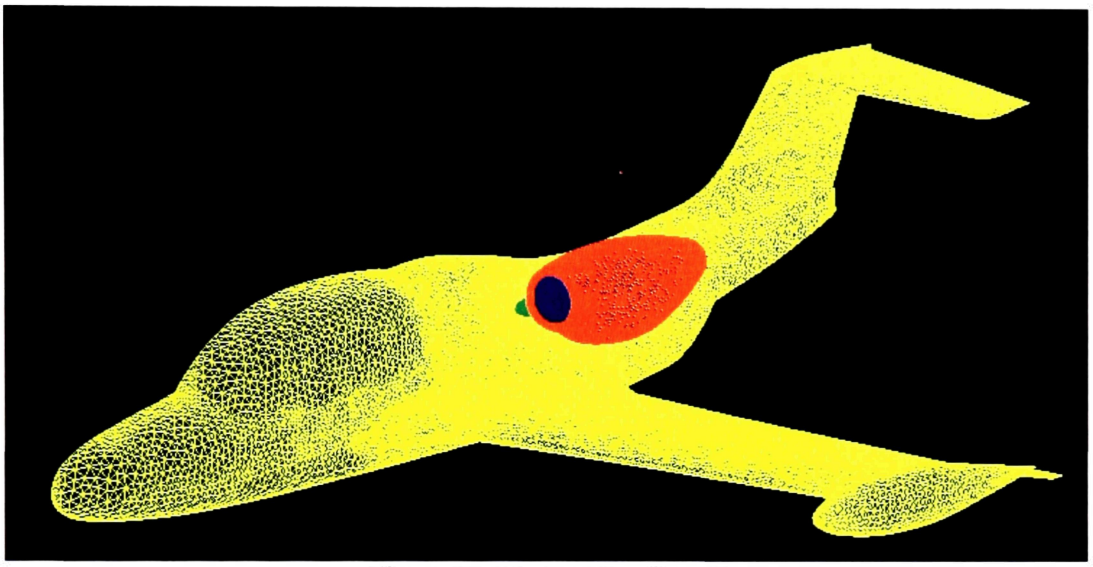

Figure 26: Mesh of the aircraft

On the figure below, one can see the pylon and nacelle meshing more in details.

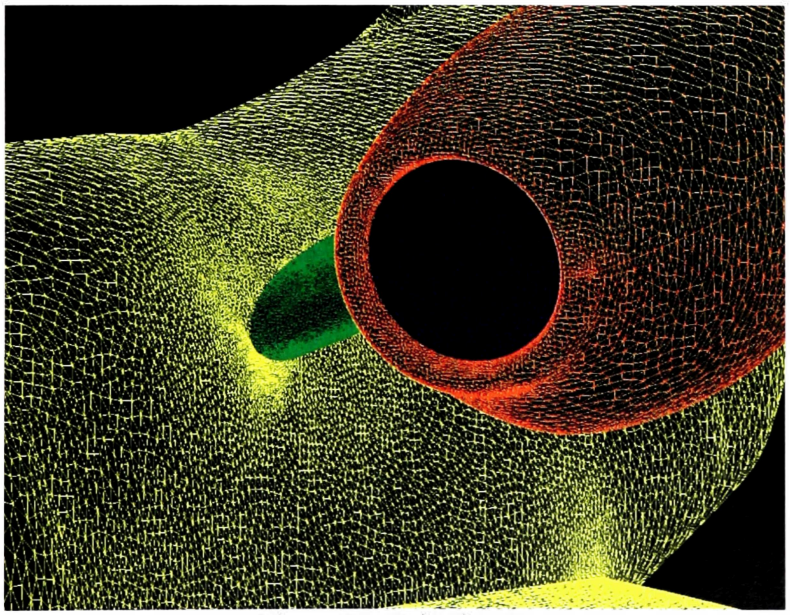

Figure 27: Grid Nacelle

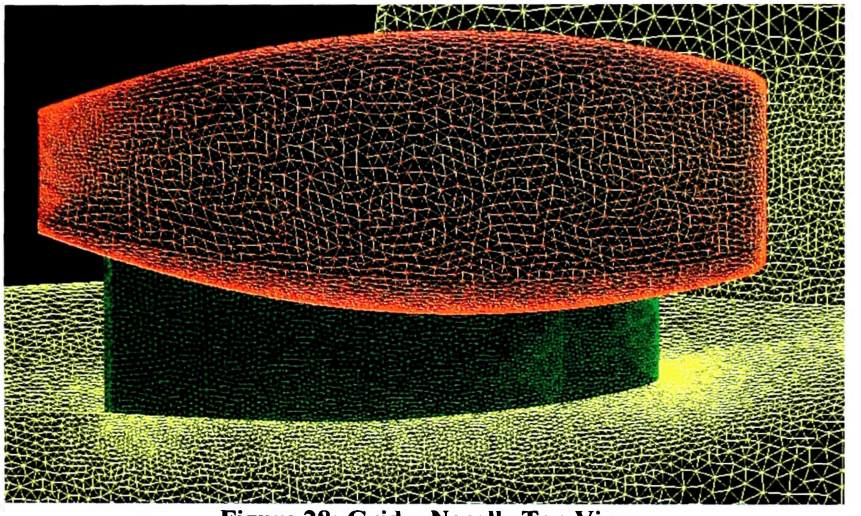

Figure 28: Grid – Nacelle Top View

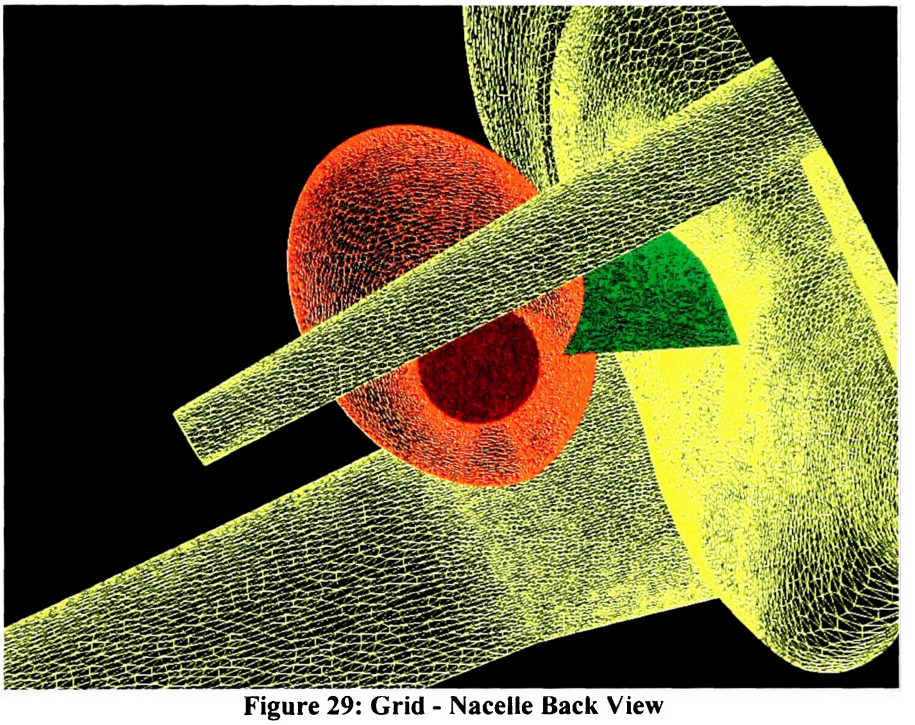

Figure 29: Grid - Nacelle Back View

3.1.2 Description of the blocks of interest

The region immediately surrounding the aircraft is split into 11 blocks.

3.1.2.1 Engine Outlet

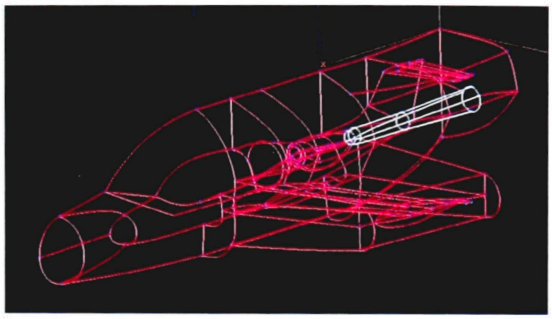

This region is a critical one as huge gradients of temperature (550 K at the exhaust versus 239 K in the free stream) are operating at the outer boundary. The shape of the cone has been adapted based on a first sample calculation, in order to match the shape of the physical jet. A finer grid has been used, especially close to the exhaust, and the boundary of the jet.

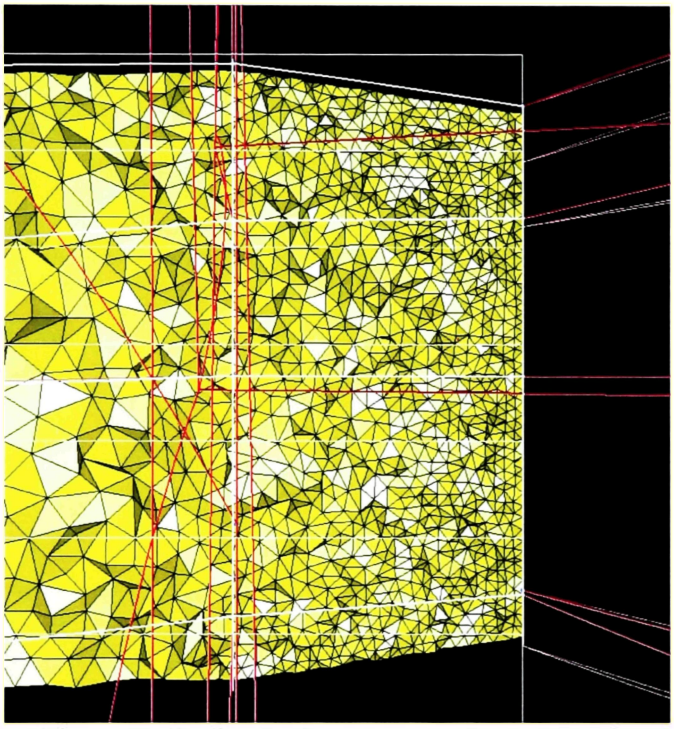

Figure 30: Engine Outlet - Constant Z cut Zoom-in

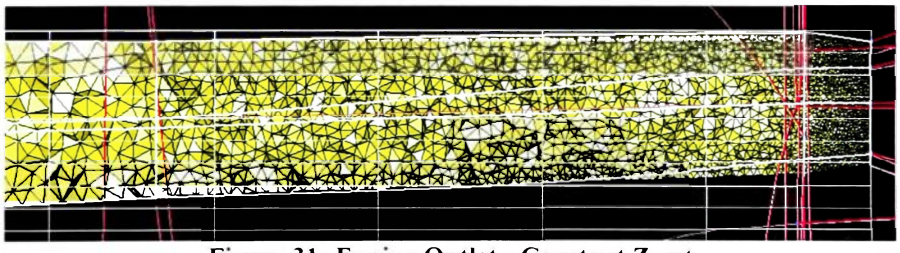

Figure 31: Engine Outlet - Constant Z cut

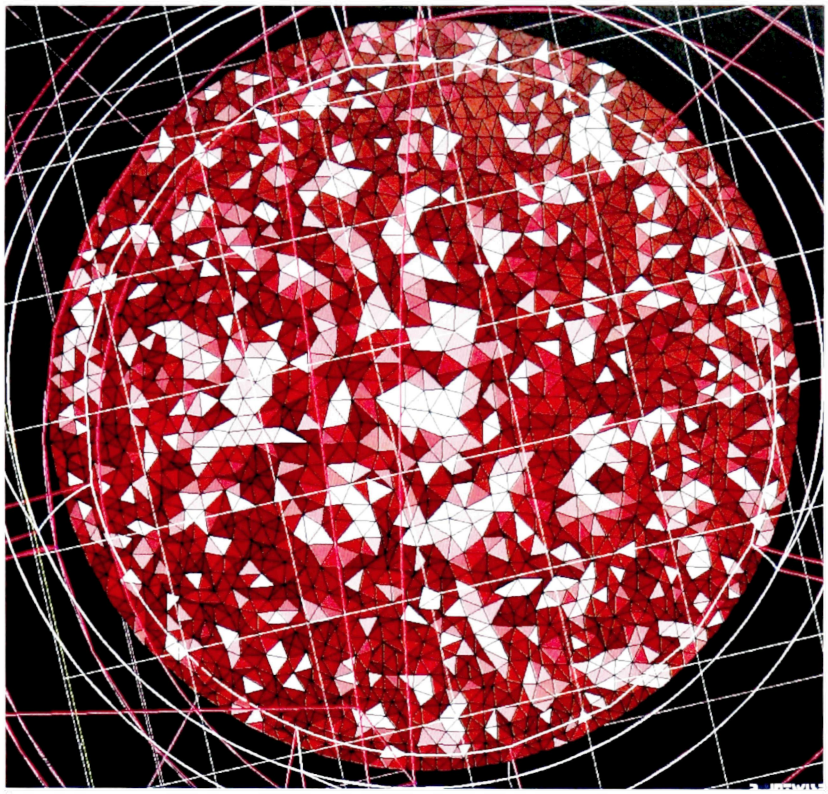

Figure 32: Engine Outlet - Constant X cut

3.1.2.2 Engine Inlet

A good accuracy is also needed at the inlet, as big gradients due to the presence of stagnation points all around the inlet of the nacelle.

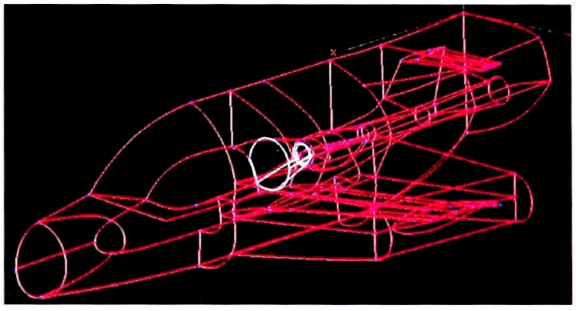

Figure 33: Engine Inlet Block

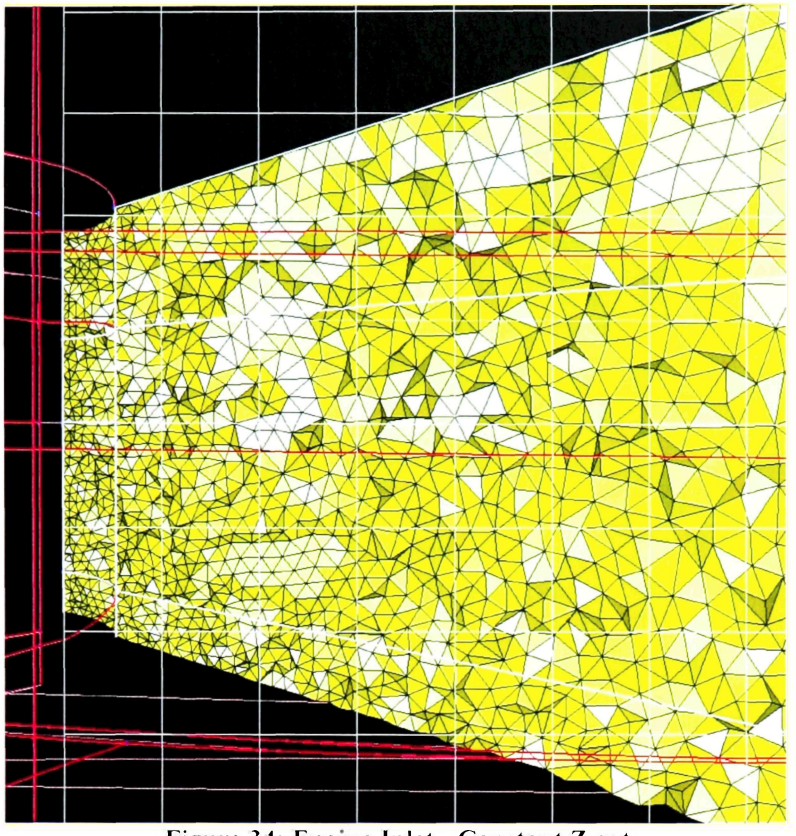

Figure 34: Engine Inlet - Constant Z cut

3.1.2.3 Nacelle Bottom

This is the most critical region, as a shock may occur between the pylon and the wing. To resolve it correctly, more grid is needed.

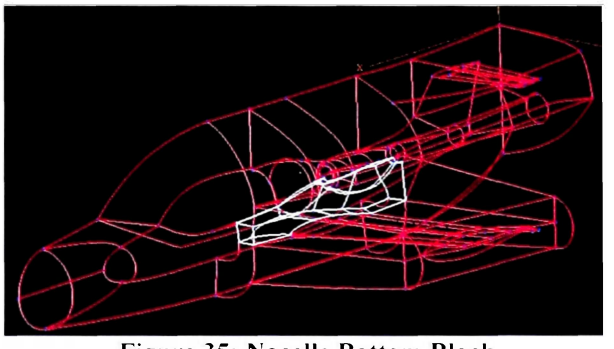

Figure 35: Nacelle Bottom Block

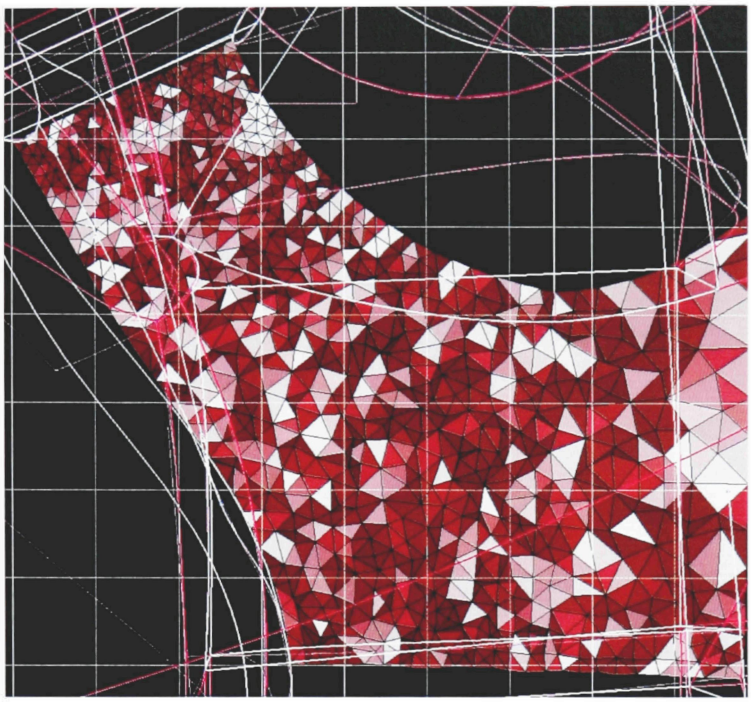

Figure 36: Bottom Nacelle - Constant X cut

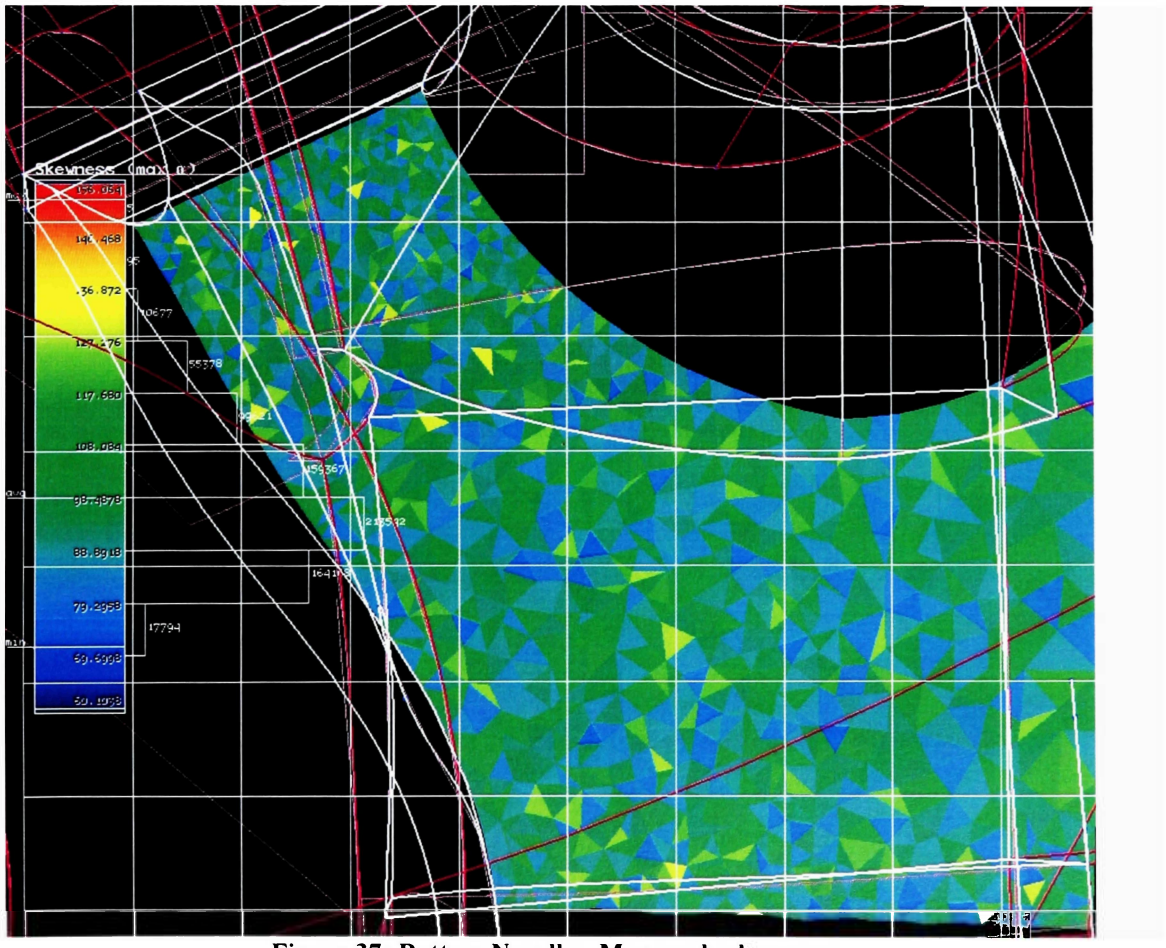

Figure 37: Bottom Nacelle - Max angle skewness

3.1.2.4 Nacelle Top

This region is also of interest as it is surrounding the upper part of the pylon and nacelle. More accuracy is needed to determine the pressure coefficients.

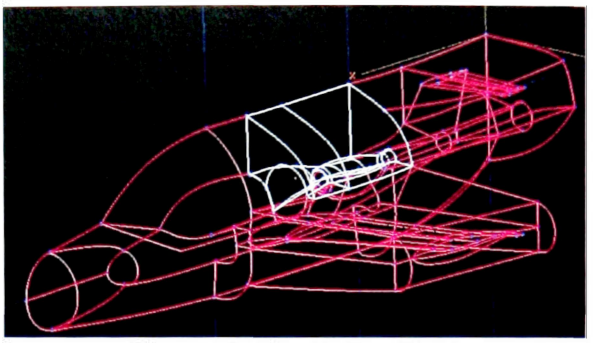

Figure 38: Nacelle Top Block

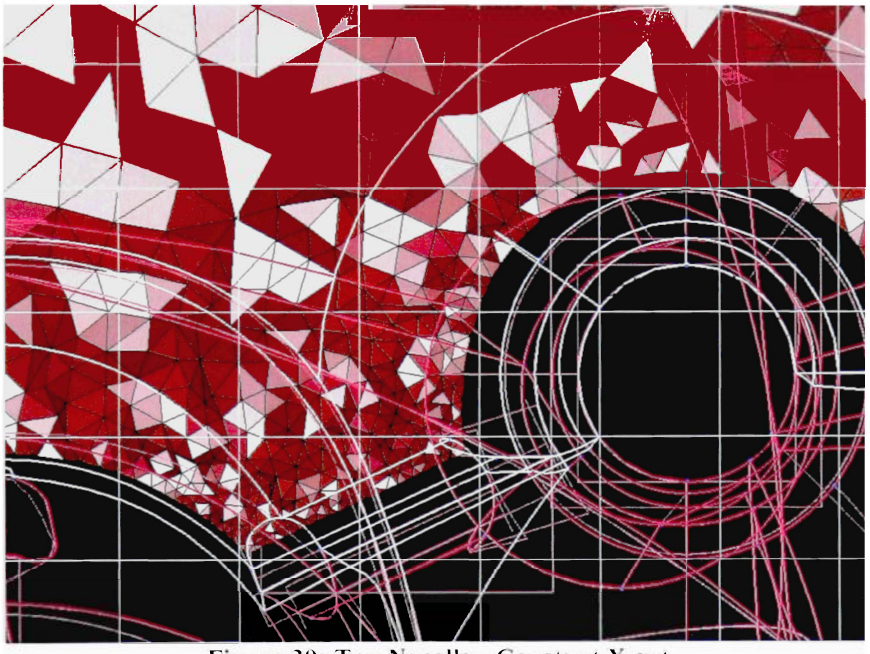

Figure 39: Top Nacelle - Constant X cut

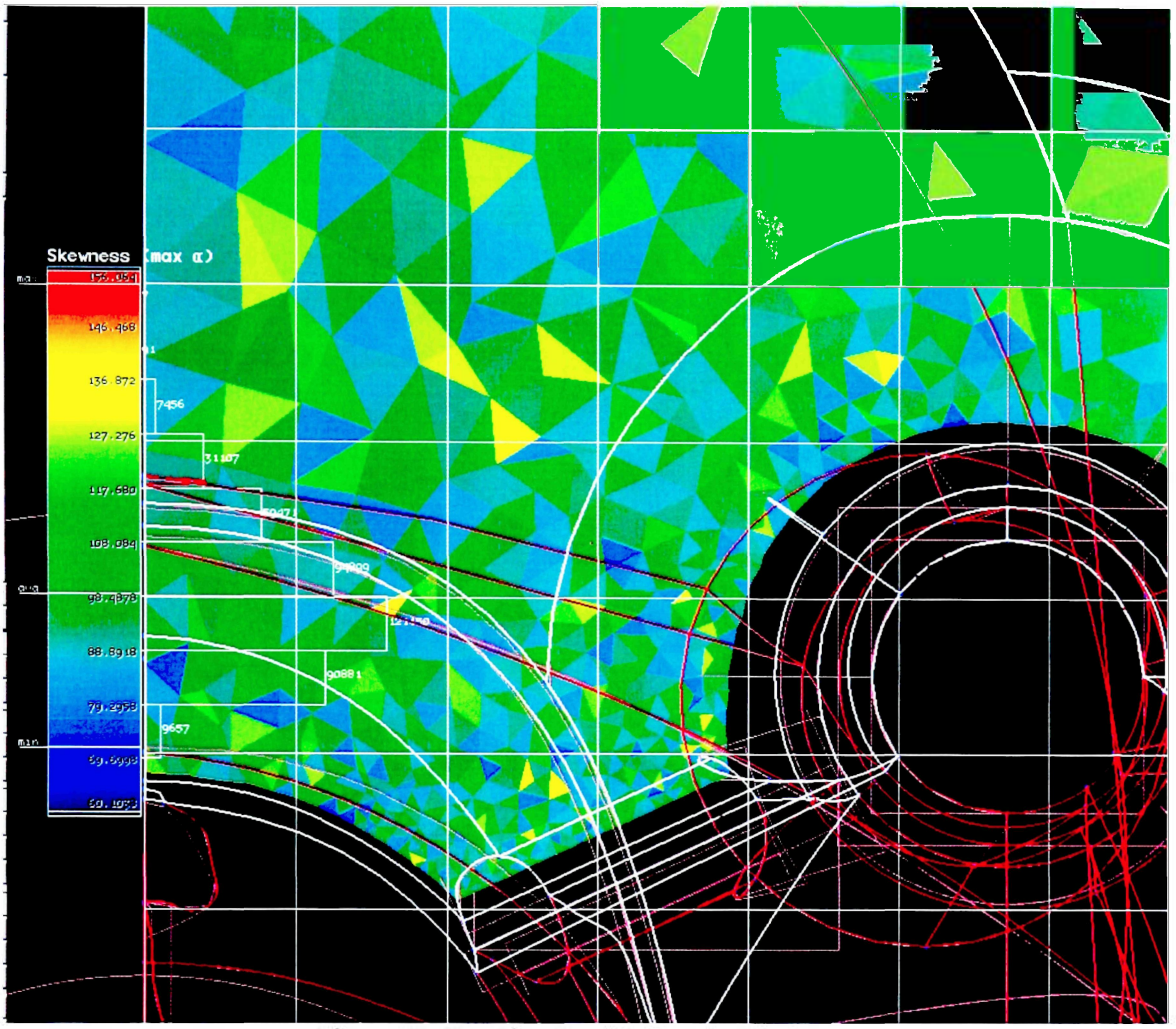

Figure 40: Top Nacelle - Max angle Skewness

3.1.2.5 Grid Statistics

An idea of the efficiency of the grid can be estimated by computing the percentage of the number of cells in the regions of interest:

Block Name	# cells	% Total
Aft Fus	**341,407**	**11%**
Canopy	99,992	3%
EngIN	**217,105**	**6.7%**
EngOUT	**323,506**	**10%**
Far 1,2,3 ,4	282,070	8.6%
NacB	**720,647**	**22%**
NacT	**414,719**	**13%**
StubB	55,284	1.5%
Tail	**221,726**	**6.7%**
Tank	45,214	1.2%
WingB	**265,291**	**8.1%**
WingT	**267,507**	**8.2%**

Table 3: Grid Characteristics

By stating the regions of interest to be the Inlet and Outlet of the nacelle, the top and bottom of it (including the pylon), the top and bottom wing, the aft fuselage (surrounding the jet mainly), and the tail, the efficiency of this grid can be estimated at 86%.

4. SOLVER: FLUENT

Fluent has been chosen for several reasons. It is a good solver for unstructured grid (the only decent one available), and is doted of a good GUI.

4.1 Parameters

The calculations have been run using Navier-Stokes equations (laminar viscous model), which are supposed to give a correct result for this type of problem. It is also a good compromise between accuracy and CPU solving time.

Fluent computes the absolute pressure using the following formula:

$$p_{abs} = p_{oper} + p_g$$

The operating pressure has been set to zero to minimize errors due to pressure fluctuations, which is really important in a high-speed compressible flow case.

The use of a pressure far-field boundary condition imposes the use of the ideal gas for the air (assumption within the Riemann invariants calculations).

Concerning the viscosity of the air being used in the flow, the Sutherland formula has been used (three coefficient method):

$$\mu = \mu_0 \left(\frac{T}{T_0} \right)^{3/2} \frac{T_0 + s}{T + s}$$

Where: T_0= 273.15 K ; $\mu 0$= 1.714 x10^{-5} N.s/m^2 ; s= 111 K.

Hence, the density and viscosity are both been made temperature-dependent.

Density Based:

As the pressure and velocity are strongly coupled in this problem (transonic flow), the density based (coupled) solver has been used.

Implicit:

The implicit scheme makes the solution converge around ten times faster for twice as much CPU solving time. An implicit scheme is also more robust than the explicit one.

Green-Gauss cell based:

Mavriplis [1] made some research about two different types of scheme proposed by Fluent: node based and cell-centered based.

According to him, a tetrahedral mesh contains five to six times more cells than nodes. Then, a tetrahedral mesh contains:

- N vertices ;
- 6N cells ;
- 7N edges ;
- 12N faces (triangles).

Basically, the cell centered approach is six times more accurate on same grid than the node based scheme. However, a node scheme on a six times finer grid is more accurate than the cell-centered scheme:

- Node scheme has 7 fluxes per control volume (7N edges);
- Cell centered scheme has 12/6=2 fluxes per control volume.

Hence, it is always better to use the cell-centered scheme on a given grid. The exception comes once the point where the solution is not changing upon the grid (the solution becomes grid independent) is reached. In this case, the node based scheme will give a better accuracy compared to the cell-centered scheme (more fluxes).

In addition, using a node based scheme may lead to instabilities at the boundaries.

Roe flux vector splitting scheme:

Fluent proposes two different types of flux vector splitting scheme: Roe and AUSM. The Roe scheme has been used in this case, as it is usually more accurate but less robust than the AUSM scheme.

Full MultiGrid (FMG) initialization:

The Full MultiGrid feature permits to start with a better initialization of the solution at a minimum cost compared to the overall computational expense. FMG initialization utilizes the FLUENT FAS Multigrid technology to obtain the initial solution. Starting from a uniform solution (after performing standard initialization), the FMG initialization procedure constructs the desirable number of geometric grid levels (five levels in this case). To begin the process, the initial solution is restricted all the way down to the coarsest level. The FAS multigrid cycle is then applied until a given order of residual reduction is obtained or the maximum number of cycles is reached. The solution is then interpolated one grid level up and the FAS multigrid cycle is applied again

between the current level all the way down to the coarsest level. This process will repeat until the finest level is reached.

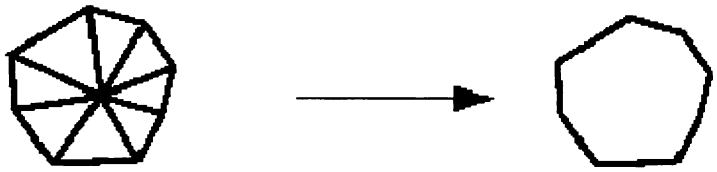

Figure 41: FAS method

Since FMG initialization does most of the work on coarse levels, this initialization procedure is computationally inexpensive and a good initial solution can be obtained in a fraction of the time spent to converge on a final solution.

The limitations of the FMG initialization method does not apply in this case (unsteady flows, turbulence model, multiphase flows).

4.2 Boundary Conditions

4.2.1 Far Field Characteristics

The following values have been used to define the pressure far-field boundary condition:

- $M_\infty = 0.7$
- $T_\infty = 239$ K
- $p_\infty = 37601$ Pa
- Unit X vector = -cos 2°
- Unit Y vector = 0
- Unit Z vector = sin 2°

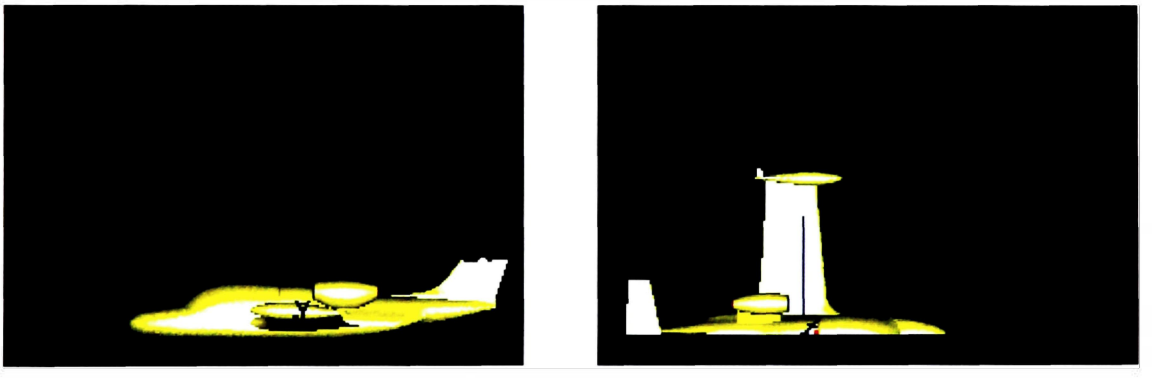

As the air is assumed ideal in this case, the ideal gas definition for the flow has been enabled. The solution is initialized from the pressure far-field conditions.

4.2.2 Engine Inlet

The engine inlet represents the surface at the inlet of the nacelle. A pressure outlet boundary condition has been used. The physical values at that BC are the same than the ones in the far field (except that the total temperature has to be used here):

- U_∞= 217 m/s
- p_∞= 37601 Pa
- $T_{0\infty}$= 262 K.

The total temperature is computed with the following formula:

$$T_0 = \left(1 + \frac{\gamma - 1}{2} M_\infty^2\right) \times T_\infty$$

Plus, a targeted mass flow rate has been set up, based on the flow characteristics and the inlet area:

$$\dot{m}_i = \rho_\infty A_i U_\infty = 0.5489 \times 0.11 \times 217 = 13.1 \text{kg/s}$$

4.2.3 Engine Outlet

The engine outlet represents the surface at the exhaust of the nacelle. A pressure inlet boundary condition has been used. The physical values at the BC have been estimated using the engine's manufacturer data, the thrust equation and the ideal gas law.

The temperature at the exhaust is assumed to be T_e= 550 K.

The thrust equation is the following:

$$\mathrm{T} = \dot{m}_i \left[(1+f)U_e - U_i\right]$$

The velocity at the inlet is the same that U_∞:

$$U_i = U_\infty = 217\, m/s$$

The fuel-to-air ratio f is assumed to be 2%:

$$f = 0.02\,\dot{m}_e = 1.02\dot{m}_i = 13.36\,kg/s$$

Hence, the velocity at the exhaust can be computed as follows:

$$U_e = \left[\frac{T_{CR}}{\dot{m}_i} + U_i\right] \times \frac{1}{1+f} = 387\,m/s$$

$$\text{where} \quad T_{TO} \simeq 6672\,N \;;\; T_{CR} \simeq 0.35\,T_{TO} = 2335\,N$$

Thrust at take-off is given by the manufacturer (1500 lbf).

The speed of sound at the exhaust can be computed as follows:

$$c_e = \sqrt{\gamma R T_e} = 470\,m/s$$

Hence, the flow at the exhaust is subsonic (M_e= 0.82).

The density can be calculated with the following formula:

$$\rho_e = \frac{\dot{m}_e}{U_e A_e} = \frac{13.36}{387 \times 0.071} = 0.4862\ \text{kg/m}^3$$

And, by using the ideal gas law:

$$p_e = \rho_e R T_e = 76747\,Pa$$

The total temperature and pressure at the exhaust are computed as follows:

$$T_{0e} = \left(1 + \frac{\gamma - 1}{2} M_e^2\right) \times T_e = 624\,K$$

$$p_{0e} = p_e + 0.5\rho_e U_e^2 = 113{,}156\,Pa$$

4.3 Sign Corrections

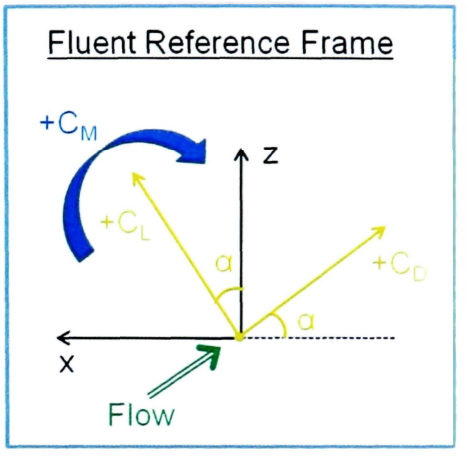

Figure 42: Forces sign convention

To compute the right forces and moments, a special attention has to be applied in order to respect the aerodynamic conventions.

Figure 40 shows the convention used with respect to the Fluent reference frame.

To define the forces computed by Fluent, the components of the unit vector in the direction of the desired force have to be defined.

Therefore, to compute the lift coefficient:

- X component = sin(α) ;
- Y component = 0 ;
- Z component = cos(α).

To compute the drag coefficient:

- X component = -cos(α) ;
- Y component = 0 ;
- Z component = sin(α).

The pitching moment coefficient (C_M) is computed about the Y-axis.

The reference values used are computed from the Far field conditions. The length used to nondimensionalize the forces is the length of the fuselage (L=10.2 m). The area used is half the wetted area of the aircraft: A= 48.85 m^2.

These reference values (length and area) have been changed to the MAC (1.9 m) and the Wing planform area (18 m^2) so that the results can be compared with the theoretical values.

5. RESULTS

5.1 Cases

Two different cases have been studied here. The first one has been done using the complete grid (with nacelle and pylon) and the second without. The same initial conditions have been used in both cases. The goal of using the two different grids was to make a better comparison of the flow over the wing with and without the nacelle.

5.1.1 Case 1: Complete grid

As previously stated, the complete grid (aircraft with nacelle and pylon) is composed of 3.25 million cells. The viscous model "Laminar" has been used (Navier-Stokes equations) with a second order accuracy. The solution has been run from a previous calculation to save time.

The solution has been iterated approximately 13,000 times with a Courant number (CFL) of 2.

To validate the results, the plots of the residuals (continuity, x momentum, y momentum, z momentum and energy equations) and the lift, drag and moment coefficients have been reported.

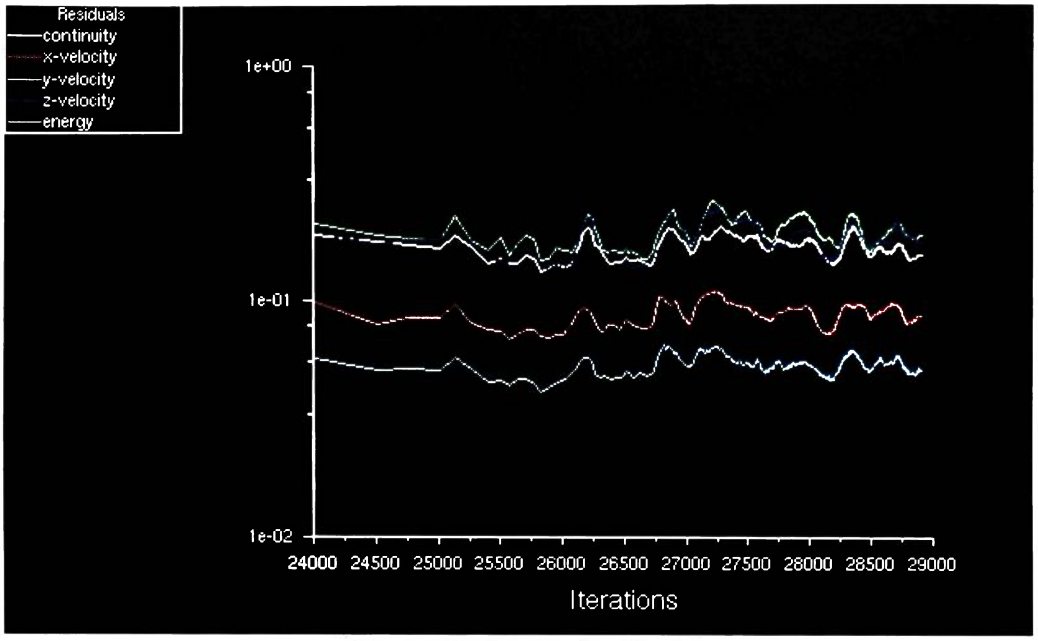

Figure 43: Case 1 - Residuals

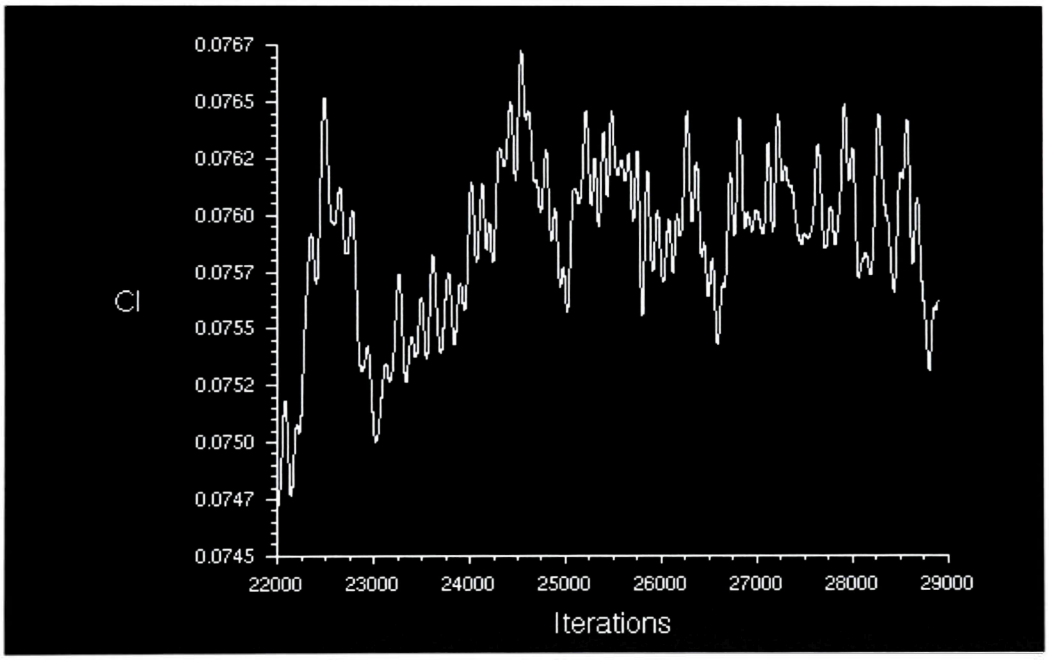

Figure 44: Case 1 - Lift coefficient

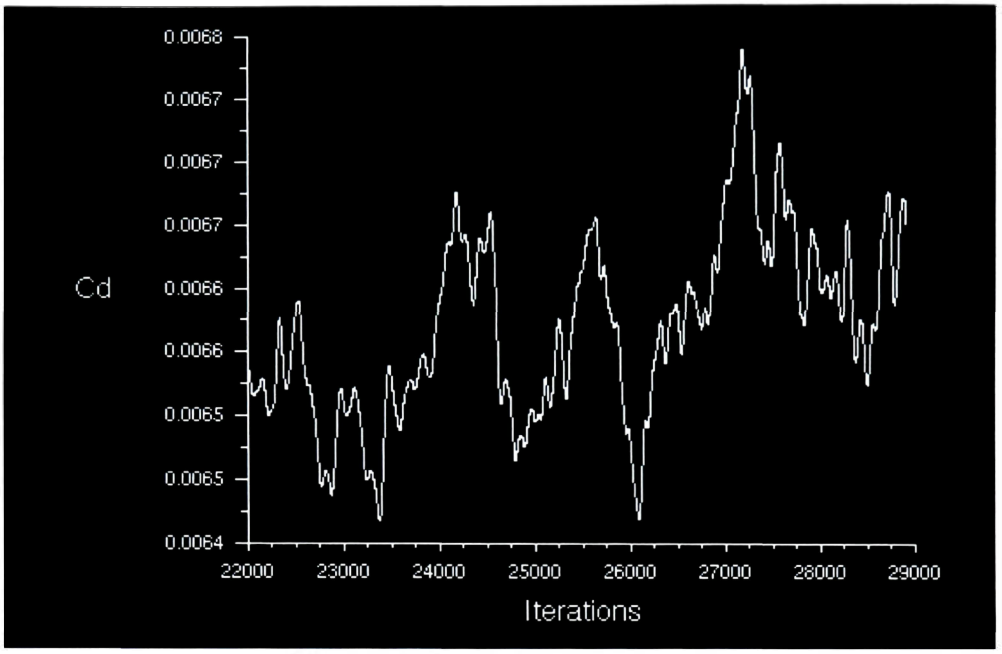

Figure 45: Case 1 - Drag coefficient

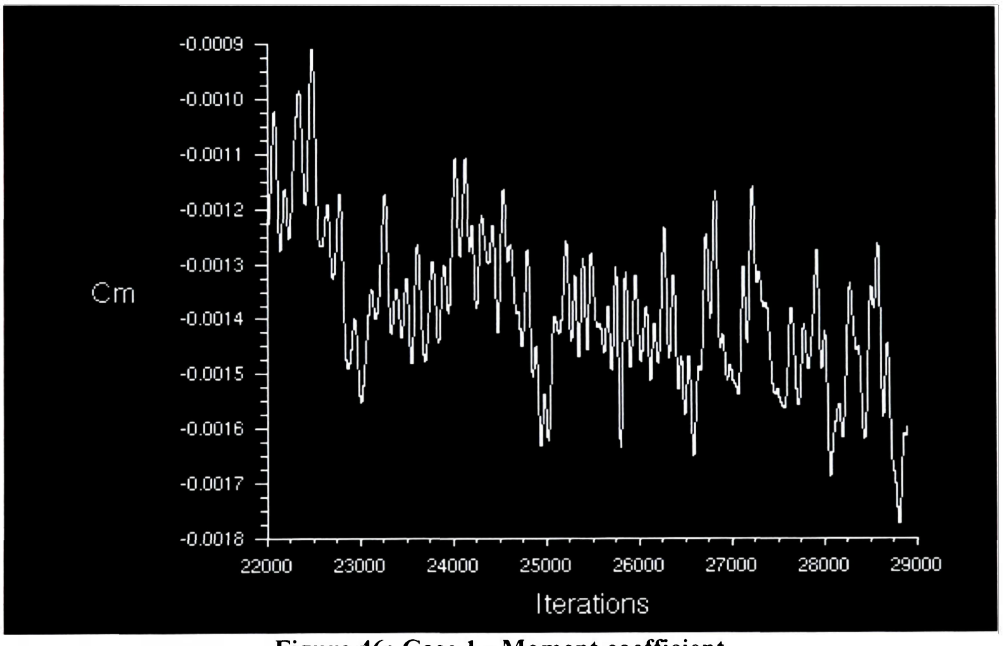

Figure 46: Case 1 - Moment coefficient

One can see that the residuals are leveled-off, meaning that the solution is converged. However, they are slightly high due to the unsteadiness of the solution (mainly because of the jet). The force and moment coefficients are oscillating within a small interval.

A good validation is to compare the results obtained from CFD to the theory. These theoretical values of lift, drag and pitching moment have been estimated applying the Raymer equations [2] on the new design. These equations are mainly based on empirical studies, and usually give a good prediction. To compare with theory, the coefficients obtained from Fluent have been computed using the same reference values than the ones used in Raymer equations: the Mean Aerodynamic Chord (MAC = 1.9 m) for the reference length and the wing planform area (S_w= 18 m²) for the reference area. As the values from CFD were oscillating, a mean value over the last 6,000 iterations for each coefficient has been taken into account.

Aerodynamic coefficients						
	C_L	% error	C_D	% error	C_M	% error
Fluent	0,2052	1.4 %	0,01996	8.1 %	-0,01592	12.2 %
Theory	0,2083	N/A	0,02173	N/A	-0,01814	N/A

Table 4: Comparison with theory

The lift coefficient obtained from CFD is very close to theory and the drag coefficient remains within the 10% error. However, the moment coefficient is a bit off (12.2%) but given the fineness of the grid and the solver parameters (laminar viscous model 2nd order), it can still be considered acceptable.

The theoretical values have been calculated using an approximation of the center of gravity position, and are, by definition, an estimation. In addition, the flow is clearly turbulent: a perfect match is then impossible.

Also, the total mass flow rate estimated by Fluent was -0.776 kg/s (should be zero for a perfect solution), which means the solution is acceptable.

To conclude, the values are close enough to validate the case.

5.1.2 Case 2: Grid without nacelle

The grid without the nacelle (aircraft only) is composed of 1.26 million cells. Basically, the same parameters have been used: "Laminar" with a second order accuracy. The solution has also been run from a previous calculation.

The calculation has been iterated approximately 11,000 times with a Courant number (CFL) of 2.4.

The following plots describe the convergence history of the residuals, the lift, drag and moment coefficients.

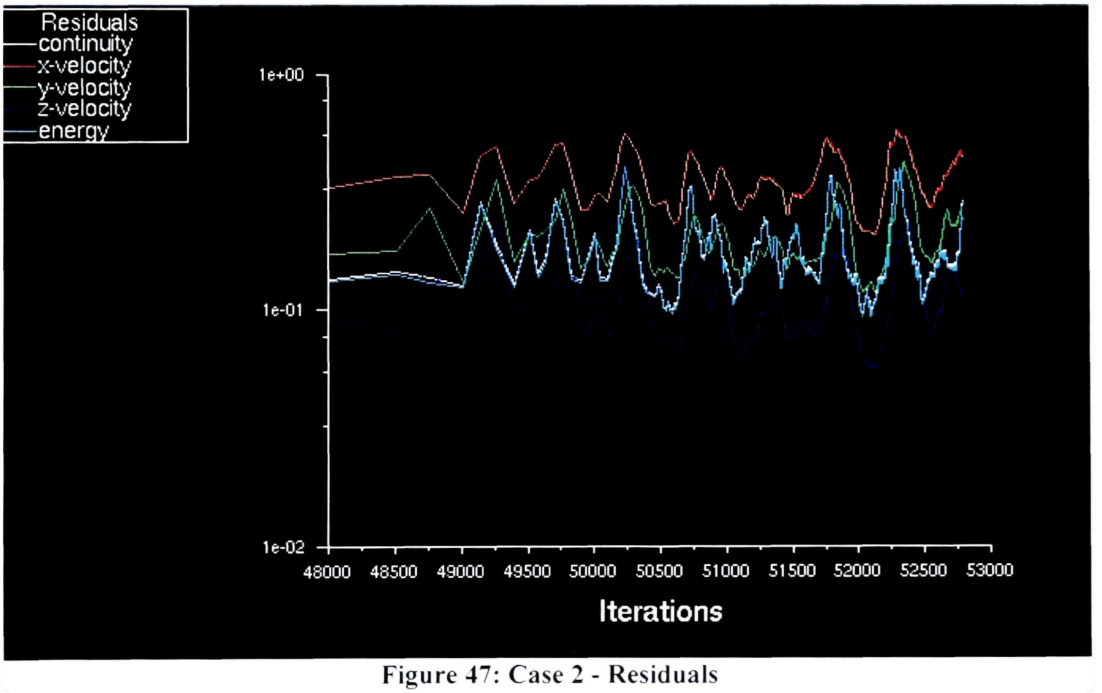

Figure 47: Case 2 - Residuals

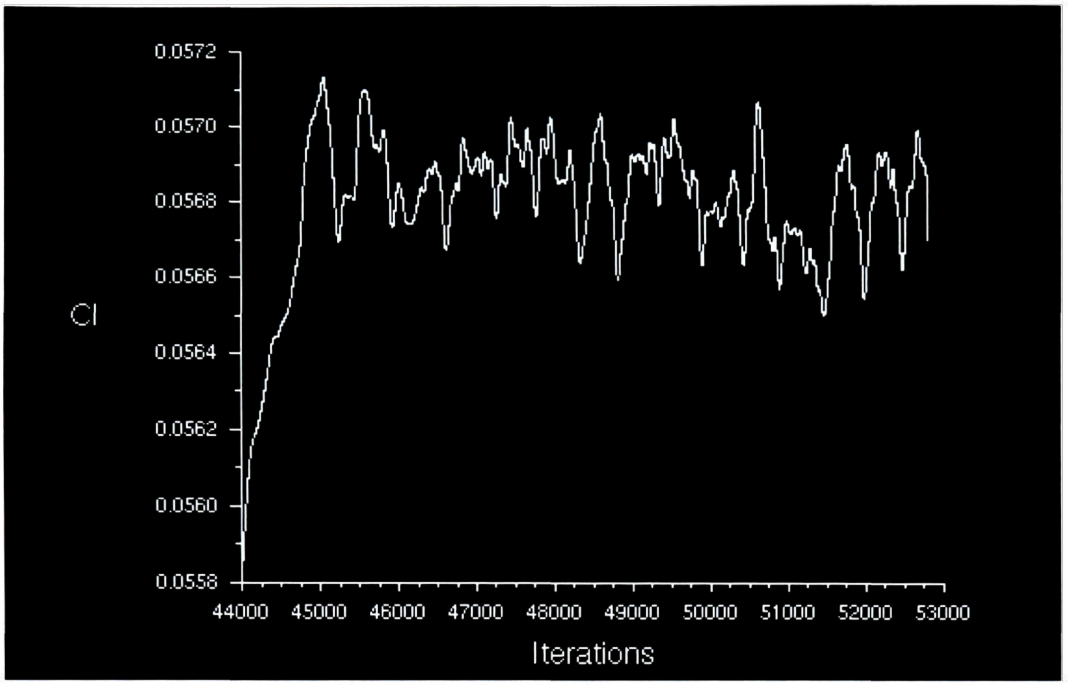

Figure 48: Case 2 - Lift coefficient

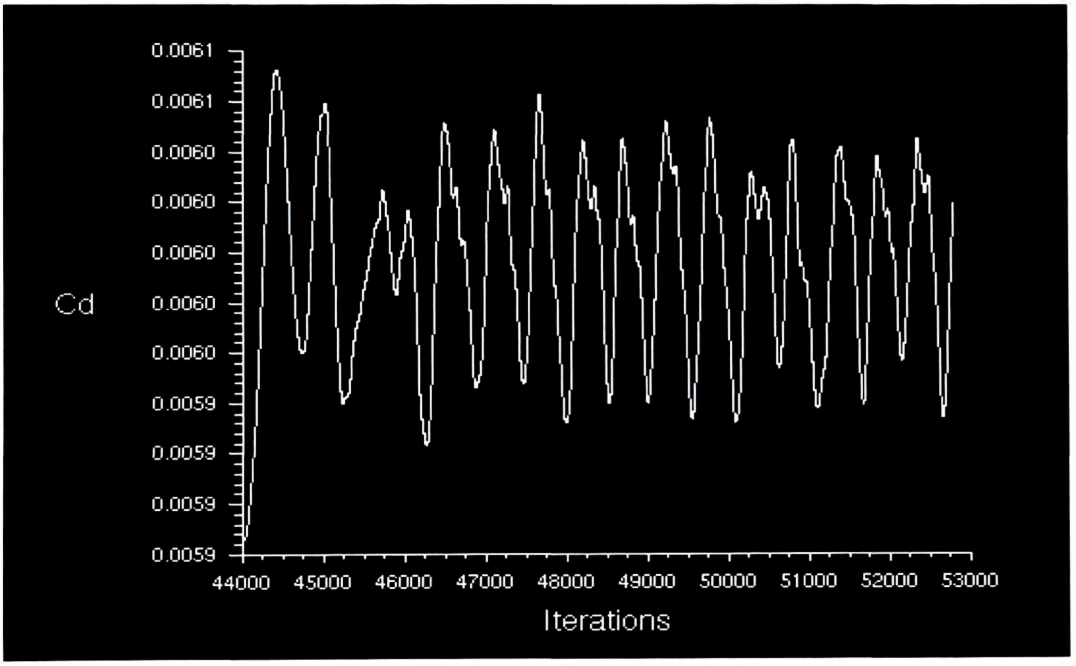

Figure 49: Case 2 - Drag coefficient

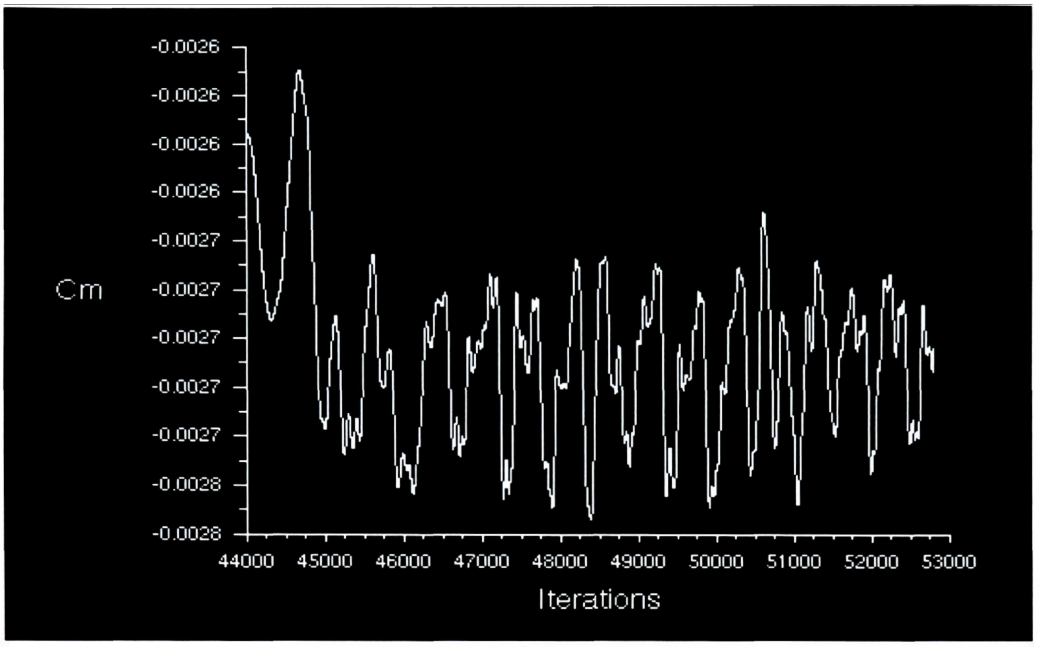

Figure 50: Case 2 - Moment coefficient

Again, one can conclude that the solution is converged, as the residuals are leveled-off.

The force and moment coefficients are also oscillating with slightly the same frequency.

5.2 Analysis

5.2.1 Streamlines

The following figures show some pictures of the complete grid solution using the streamline feature in FieldView.

Figure 51: Mach number streamlines

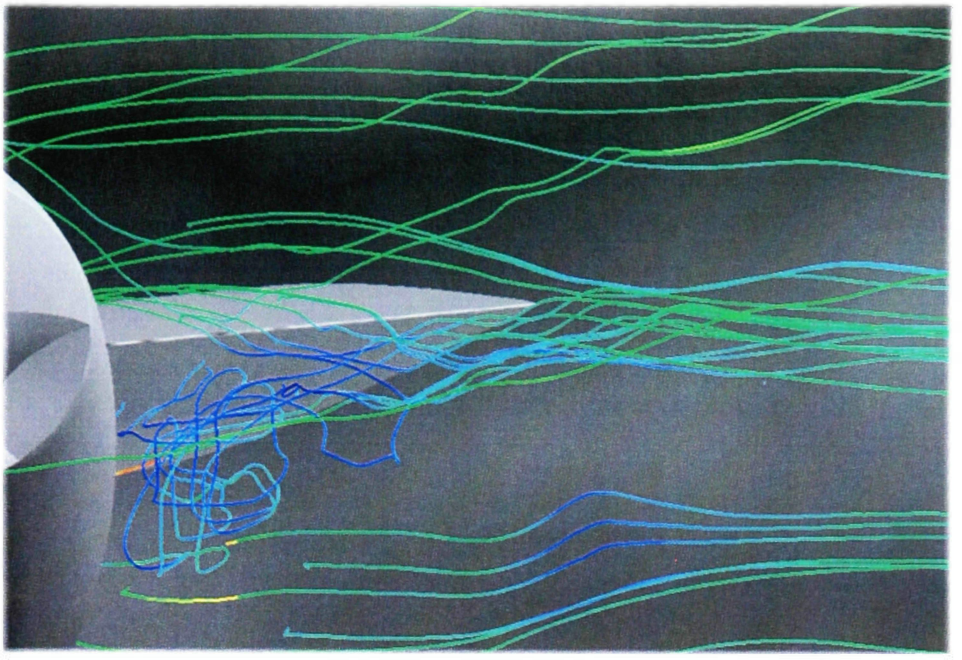

Figure 52: Vortices forming behind the pylon

Vortices are forming in the region between the trailing edge of the pylon and the nacelle. These vortices greatly increase the drag, but can be avoided by modifying the connecting shape between the pylon and nacelle.

5.2.2 Contours

To have a better understanding of the nacelle influence, an observation plane parallel to the XZ plane has been defined. It is located in such a way that the flow around the wing, the nacelle and the tail can be analyzed at the same time. The definition of this observation plane is illustrated in Figure 51.

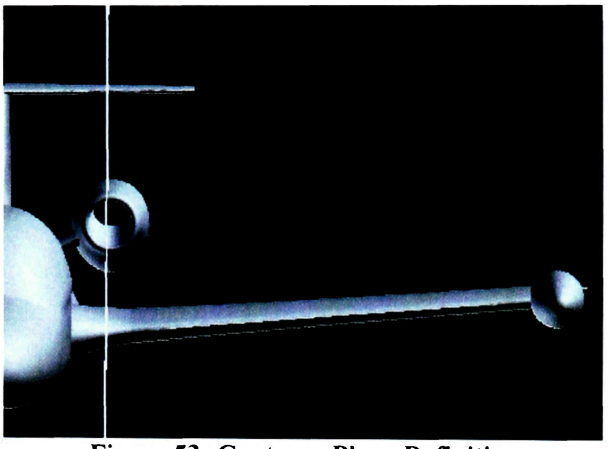

Figure 53: Contours Plane Definition

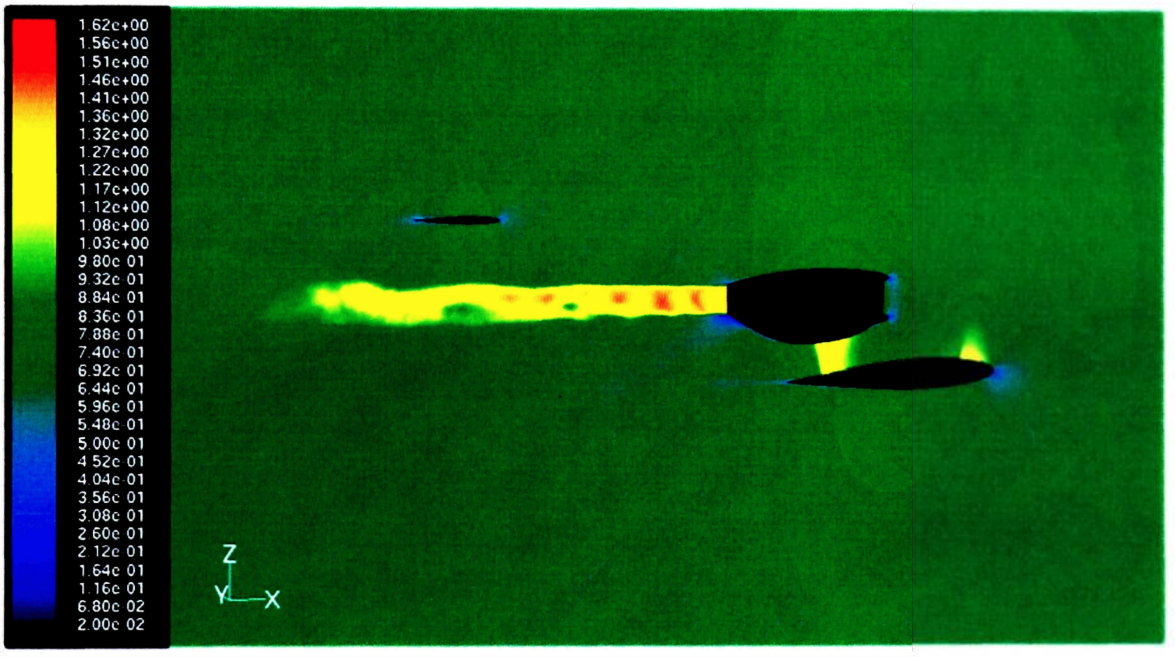

Figure 54: Mach number contours – Observation Plane

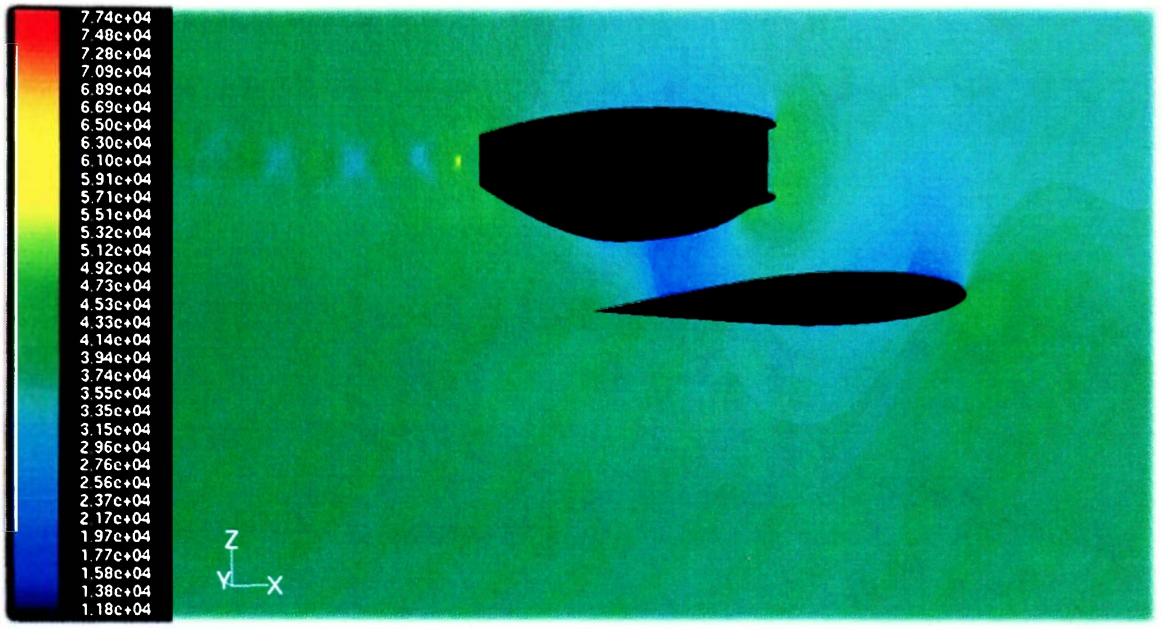

Figure 55: Static pressure contours - Observation Plane

One can note that in Figure 52 and Figure 53 a shock between the nacelle and the wing is clearly forming. A close-up of this region is illustrated in Figure 54 and 55.

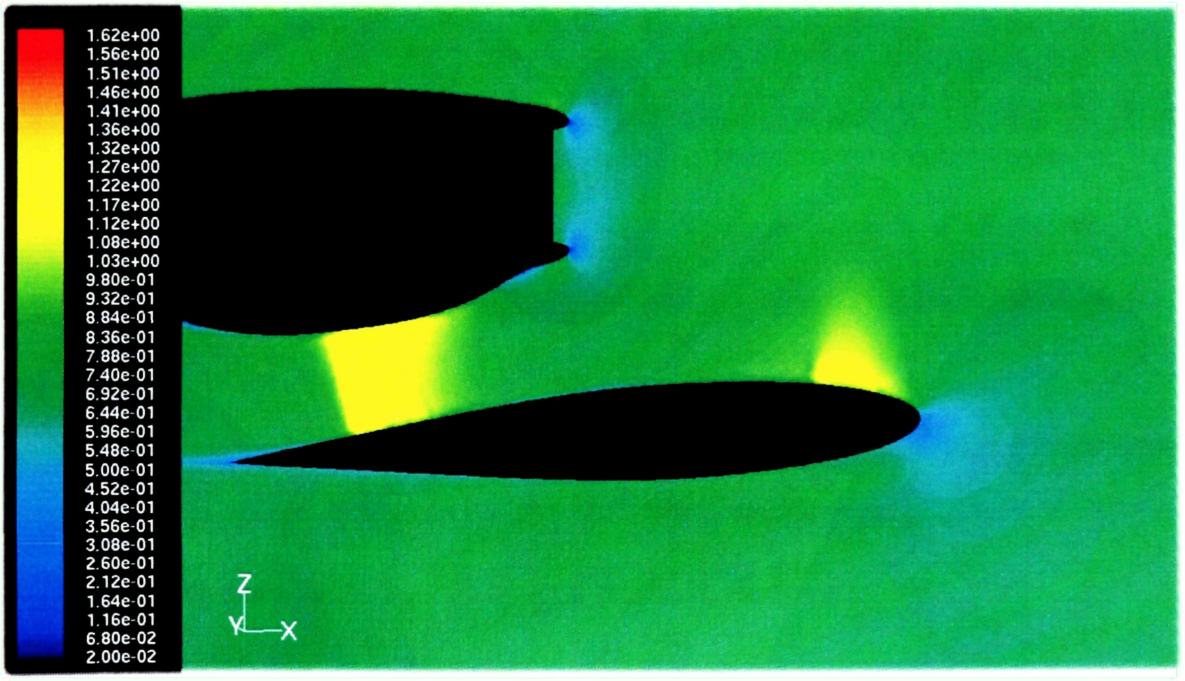

Figure 56: Mach number contours - Shock between Wing and Nacelle

Figure 54 illustrates the flow between the nacelle and the wing. One can see that the flow accelerates up to a Mach number of 1.3 and then a shock wave occurs. The nacelle is actually acting as a convergent nozzle.

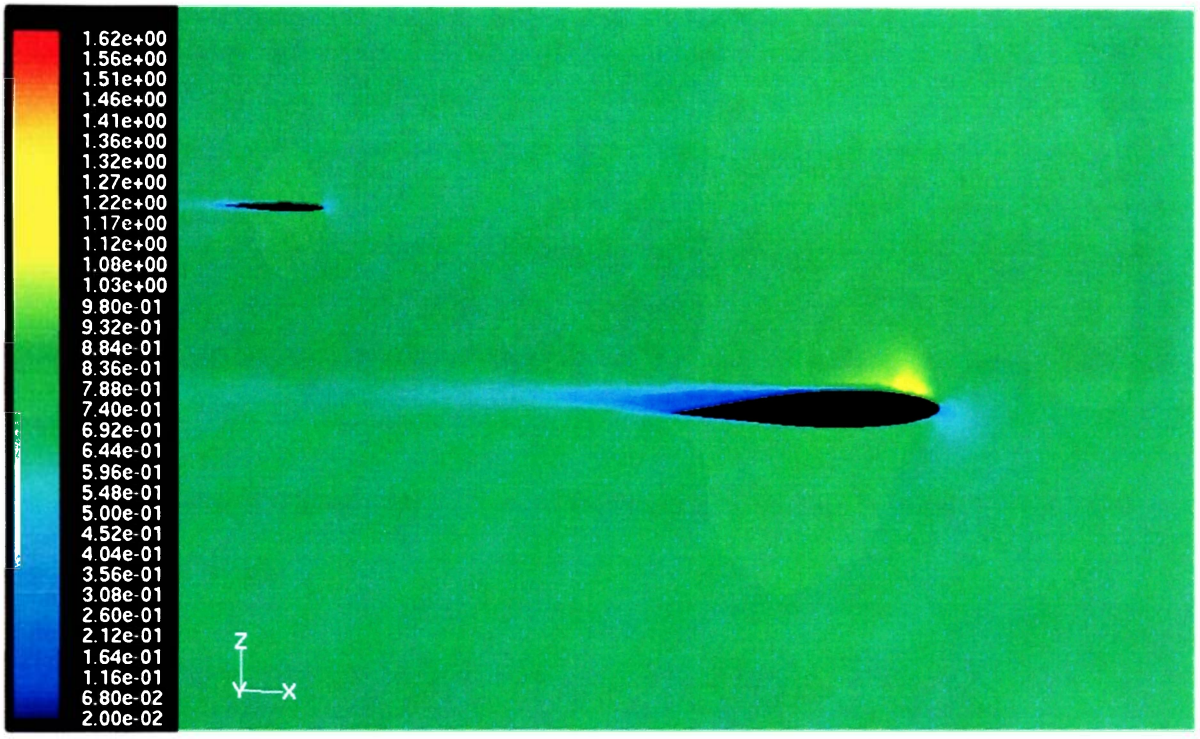

Figure 57: Mach number contours - Observation plane - Aircraft without Nacelle

Figure 55 illustrates the flow over the wing in the observation plane of the aircraft without the nacelle. The shock occurring with the nacelle does not exist without. Therefore, the nacelle is fully responsible for the shock forming.

This figure also depicts the detachment of the flow over the wing, starting approximately at 50% chord length. This detachment disappears in presence of the nacelle.

Figure 56 describes the static pressure contours on the aircraft itself.

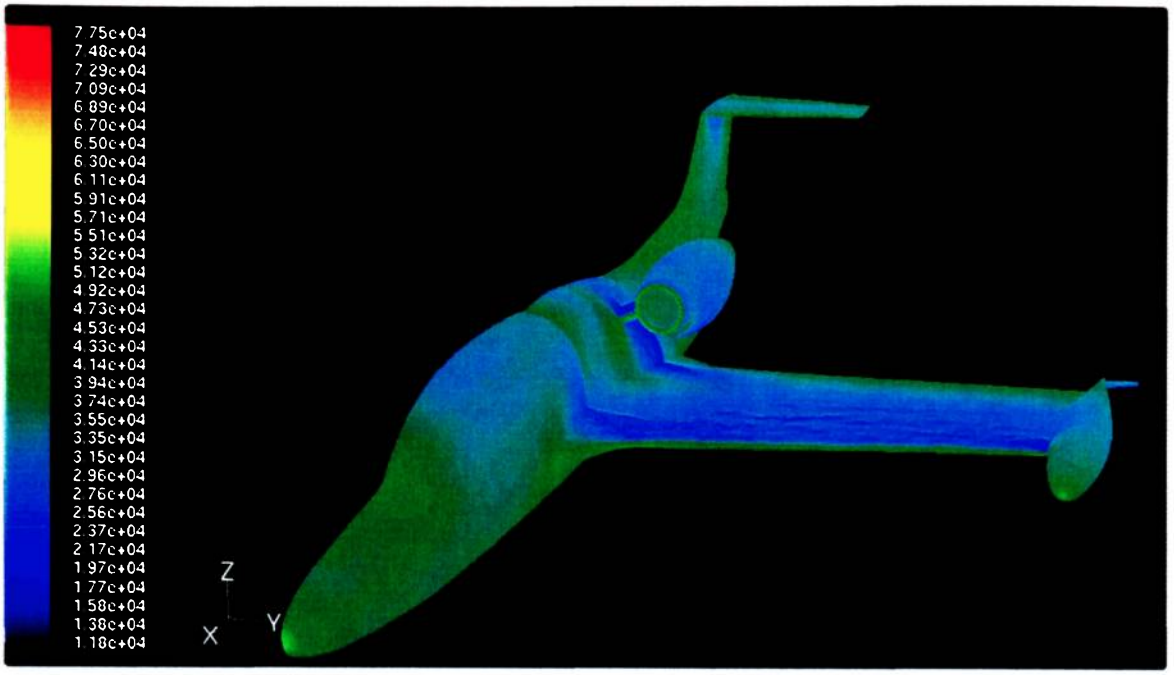

Figure 58: Static pressure contours on the aircraft

The following figures illustrate more in details the location of the shock created by the presence of the nacelle.

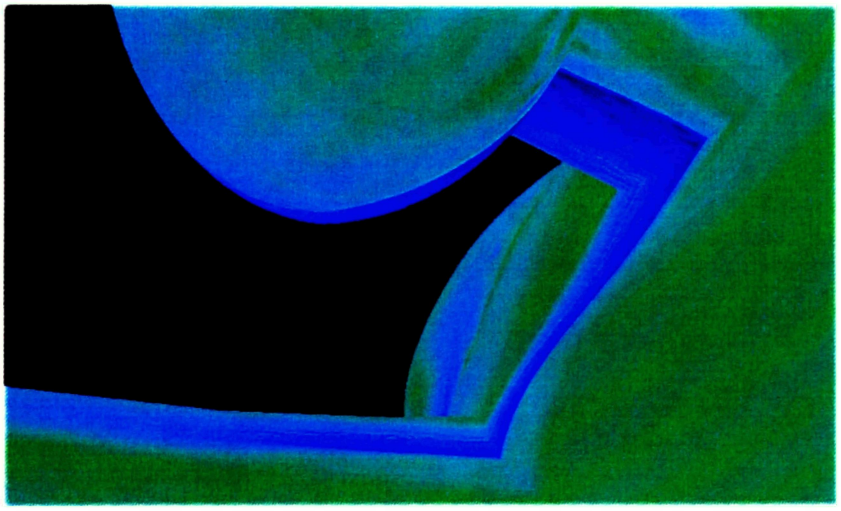

Figure 59: Static pressure contours - Nacelle Back View

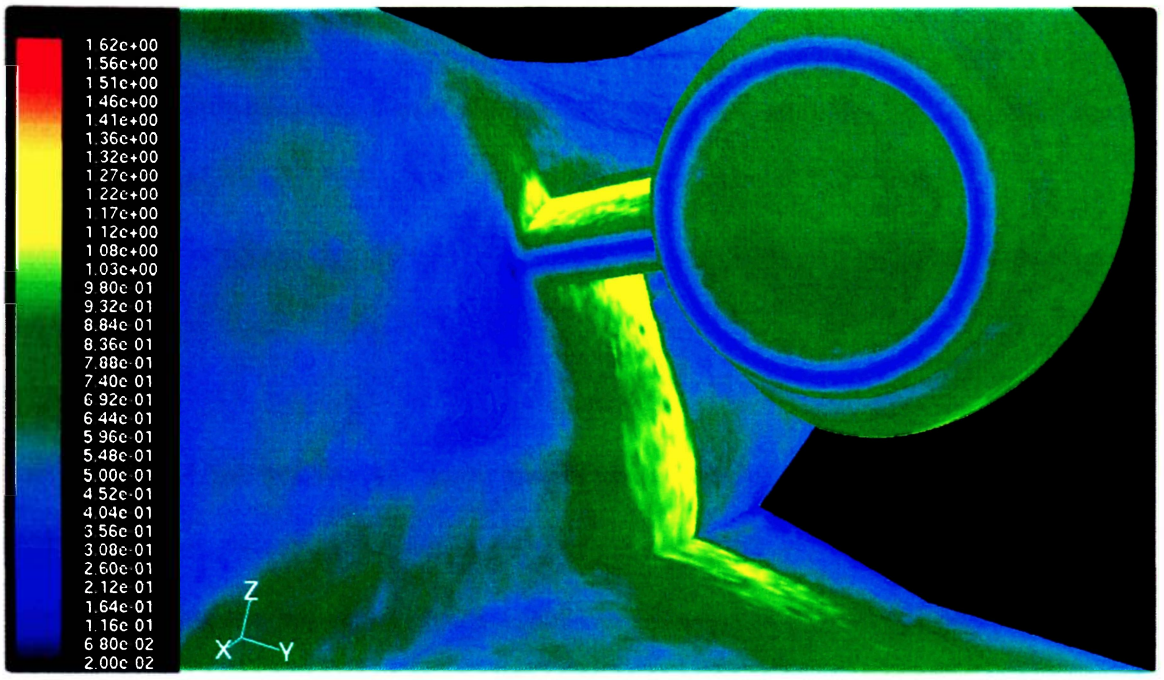

Figure 60: Mach number contours - Nacelle front view

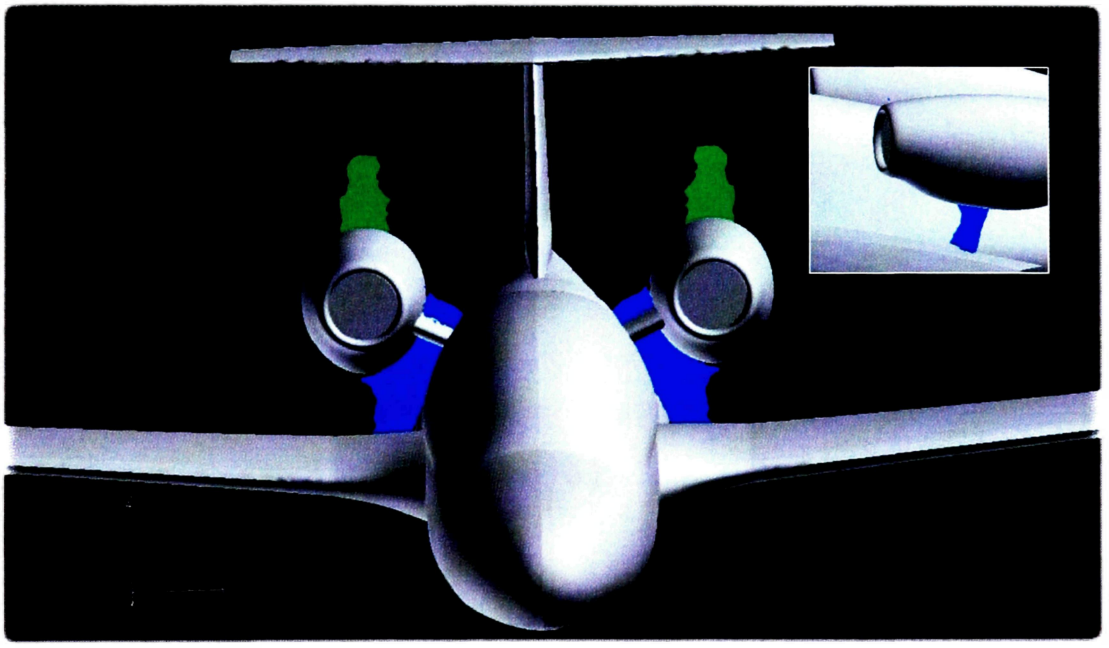

Figure 61: Iso-surface Mach number (M=1.2)

Figure 59 shows that another shock occurs on the upper surface of the pylon, which can also be seen on Figure 58.

6. CONCLUSIONS

The goal of this thesis was to illustrate the influence of the nacelle and pylon on the aerodynamics of the MS 760C ParisJet IV using Computational Fluid Dynamics.

After validation of the model based on the comparison of the lift, drag and moment coefficients with theory, the results have been processed.

The most critical issue is the downwash effect. Indeed, the wing downwash, the downward motion of the mass of air accelerated by the wing, and the position of the nacelle close to the wing, produce shock waves at the pylon. There are two shocks forming, one between the wing and the nacelle, and a second on the upper surface of the pylon.

These shocks have to be avoided, as they affect the performance of the aircraft. Indeed, they cause flow to separate, creating vortices at the trailing edge of the pylon, generating noise, vibration and more drag (wave drag).

A solution could be to move the nacelle aft enough, such that the flow accelerating from wing downwash would not be coupled with the flow accelerating under the nacelle. An alternative would be to move the nacelle upward for the same reasons.

In addition, the nacelle should be located further from the fuselage to avoid the shock over the pylon.

To conclude, the location of the nacelle is not a good choice as it affects the performance of the aircraft. The next study would be to find the best position of the nacelle to avoid shocks due to wing downwash, and try different pylon design.

REFERENCES

[1] Mavriplis, Dimitri J., "Unstructured Mesh Discretizations and Solvers for Computational Aerodynamics", AIAA 2007-3955, 2007.

[2] Raymer, Daniel. P., "Aircraft Design: A Conceptual Approach" 4th edition, AIAA, 2006.